New spectroscopic data, spin-orbit functions, and global analysis of data on the $A\,^1\Sigma_u^+$ and $b\,^3\Pi_u$ states of Na_2

P. Qi, J. Bai, E. Ahmed, A. M. Lyyra, and S. Kotochigova
Physics Department, Temple University, Philadelphia, Pennsylvania 19122-6082

A. J. Ross and C. Effantin
Laboratoire de Spectrométrie Ionique et Moléculaire (UMR 5579 CNRS - Université Lyon 1), 43 Boulevard du 11 novembre 1918, 69622 Villeurbanne Cedex, France

P. Zalicki
KLA-Tencor, 160 Rio Robles, San Jose, California 95134

J. Vigué
Laboratoire Collisions, Agrégats, Réactivité (UMR 5589, CNRS - Université Paul Sabatier, Toulouse 3) IRSAMC, 31062 Toulouse Cedex 9, France

G. Chawla and R. W. Field
Department of Chemistry 6-219, Massachusetts Institute of Technology, Cambridge, Massachusetts 02139

T.-J. Whang
Department of Chemistry, National Cheng Kung University, Tainan, Taiwan 70101, Republic of China

W. C. Stwalley
Department of Physics, University of Connecticut, Storrs, Connecticut 06269-3046

H. Knöckel and E. Tiemann
Institut für Quantenoptik, Universität Hannover, Welfengarten 1, 30167 Hannover, Germany

J. Shang and L. Li
Department of Physics, Tsinghua University, Beijing 100084, China and Key Laboratory of Atomic and Molecular Nanosciences, Tsinghua University, Beijing 100084, China

T. Bergeman
Department of Physics and Astronomy, SUNY, Stony Brook, New York 11794-3800

(Received 5 March 2007; accepted 15 May 2007; published online 23 July 2007)

The lowest electronically excited states of Na_2 are of interest as intermediaries in the excitation of higher states and in the development of methods for producing cold molecules. We have compiled previously obtained spectroscopic data on the $A\,^1\Sigma_u^+$ and $b\,^3\Pi_u$ states of Na_2 from about 20 sources, both published and unpublished, together with new sub-Doppler linewidth measurements of about 15 000 $A \leftarrow X$ transitions using polarization spectroscopy. We also present new *ab initio* results for the diagonal and off-diagonal spin-orbit functions. The discrete variable representation is used in conjunction with Hund's case *a* potentials plus spin-orbit effects to model data extending from $v=0$ to very close to the $3\,^2S+3\,^2P_{1/2}$ limit. Empirical estimates of the spin-orbit functions agree well with the *ab initio* functions for the accessible values of R. The potential function for the A state includes an exchange potential for $S+P$ atoms, with a fitted coefficient somewhat larger than the predicted value. Observed and calculated term values are presented in an auxiliary (EPAPS) file as a database for future studies on Na_2. © *2007 American Institute of Physics*.
[DOI: 10.1063/1.2747595]

I. INTRODUCTION

There are several reasons for reexamining the spectroscopic data on the lowest excited states, $A\,^1\Sigma_u^+$ and $b\,^3\Pi_u$, of the Na_2 molecule. First, there currently is widespread interest in producing ultracold ground state molecules,[1] and there are advantages in starting with laser-cooled atoms. Subsequent steps of photoassociation and Raman transfer to the ground state require accurate knowledge of excited state level structure. Second, these lowest excited states provide the most widely used pathways to higher states, and levels with mixed singlet-triplet character are of particular interest as "window states."[2] For any experiment using these lowest excited states, it is essential to have accurate term values and to know the composition of the eigenstates of interest. Third, the renewed interest in photoassociation and excitation of alkali molecules for diverse reasons has raised general questions about how to model spin-orbit functions and Born-Oppenheimer potentials, including the exchange and dispersion terms. For such questions, Na_2 is a valuable test case because it is relatively simple, with relatively small spin-orbit effects, and also the experimental data is most abundant. In view of the above, in this study we have compiled

fragmentary published and unpublished information together with extensive new sub-Doppler measurements of $A \leftarrow X$ transitions to assemble a comprehensive picture of these states. New *ab initio* spin-orbit functions play an essential role in the analysis.

The $A\ ^1\Sigma_u^+$ state of Na_2 first attracted interest because of its unexpectedly robust magnetic rotation spectrum (MRS),[3,4] which contrasted with predictions for a pure $^1\Sigma_u^+$ state, which would have negligible magnetic moment. With the help of Mulliken's survey of molecular orbital structure of diatomic molecules,[5] the observed MRS was attributed to perturbations by a slightly lower-lying $^3\Pi_u$ state.[4] Vibrational numbering of the A state was determined in Ref. 4, and information on the $^3\Pi_u$ perturber was deduced by Carroll.[6] Vibrational numbering of the b state was established much later by Li *et al.*[7]

More detailed study of the perturbations in the Na_2 $A \leftarrow X$ spectrum was apparently carried out first by Kusch and Hessel[8] in 1976, based on absorption spectra obtained with a grating spectrograph. They reported detailed rotational structure near perturbation crossings in $v=0$ and 1 of the A state, but did not report interaction parameters.

Since the earliest days of laser spectroscopy, there have been many high quality observations of restricted sets of levels of the Na_2 A and b states, depending on the resources of each laboratory. The first laser spectroscopic study of the Na_2 A state by Kaminsky in Schawlow's laboratory reported (also in 1976) the observation of some 114 $A \leftarrow X$ spectral lines.[9,10] It was noted in Ref. 10 that one level was perturbed. Slightly later Engelke *et al.*,[11] Atkinson *et al.*,[12,13] and Shimizu and Shimizu[14] observed transitions to various levels of the b state, using lasers and molecular beams. $A \sim b$ coupling parameters were extracted, and the b state spin-orbit splitting was observed.

A systematic study of $A \sim b$ perturbations in low vibrational levels of the A state was presented by Effantin *et al.*[15] and Babaky.[16] They used Fourier transform spectroscopy to resolve emission from the (2) $^1\Sigma_g^+$ state. All-optical triple resonance[17] and perturbation-facilitated optical-optical double resonance methods allowed Whang *et al.*[18,19] to obtain information on lower and higher vibrational levels of the b state. More recently, Zalicki *et al.*[20] obtained precision laser molecular beam data on levels of the $b\ ^3\Pi_u$ state that perturb the lower vibrational levels of the A state. Notable among other studies cited in Sec. II are those by Chawla and co-workers,[21,22] who measured two rotational levels in each of the A state vibrational levels $v=62-105$ by modulated gain spectroscopy, and by Tiemann *et al.*,[23] who excited stepwise via $X(v=31)$ up to the dissociation limit.

There is some urgency in making the present compilation because some of the raw spectroscopic data predate the era of electronic information storage and are available only as hard copy output, or as handwritten lists, which are in danger of being lost forever (as appears to be the case for some of the raw spectroscopic data associated with several of the sources listed below). A comprehensive survey is also useful in exposing gaps in the spectroscopic information. In fact, gaps in the original data for this survey inspired a succession of efforts to supplement the available data, as discussed below. These efforts culminated in a comprehensive study of the Na_2 $A \leftarrow X$ absorption spectrum using polarization spectroscopy to provide sub-Doppler linewidths for molecules in a heat pipe oven.[24] The assignment of some 15 000 transitions (for 13 500 lines) obtained by this means was facilitated first by retrieving handwritten tables of line positions used for Ref. 15, and second by an extensive absorption spectrum of the $A \leftarrow X$ bands, in addition to the other data available at the time.

Recent developments make a global analysis possible. (1) A direct fit to analytic potential functions in place of a fit to Dunham parameters using Rydberg-Klein-Rees (RKR) procedures eliminates the semiclassical approximation and is less subject to divergence and instability at large R values. Similar approaches have been used recently by many authors including those of Refs. 25–29. For the models used here, it is thereby easier for the "short-range" potential to extend into the region in which there is only a small overlap of the atomic wave functions. (2) In place of Numerov or other methods for obtaining individual eigenfunctions for a band-by-band analysis, it is now possible to obtain eigenvalues by matrix diagonalization of a Hamiltonian for coupled potentials. The discrete variable representation (DVR) [also known as the Fourier Grid Hamiltonian (FGH) method][30–32] is used here as in Refs. 27 and 29. This numerical method can be used to take into account coupling effects between entire manifolds of discrete and continuum states. In heavier alkali dimers, for which spin-orbit coupling functions increase in magnitude, this method or the equivalent becomes essential. A two-channel version of the DVR/FGH approach was, in fact, applied to the A and b states of Na_2 in 1995,[32] with fewer experimental data available than in the present work. To reduce the required number of mesh points, the mapped FGH method[33,34] has been used, as well as analytic scaling,[35] which we adopt here. In a sense, FGH/DVR methods present a new paradigm for modeling diatomic spectra, and this study represents another test case.

The spin-orbit functions, diagonal and off-diagonal, are clearly essential in this analysis. In the earlier stages of this work, we were able to extract empirical information on spin-orbit functions near $R=R_e$ of the b state, and near the potential crossing point, R_x, between the A and $b\ ^3\Pi_{0u}$ states, using also the known limits at large R consistent with the Na $3\ ^2P$ fine structure splitting. Eventually, *ab initio* functions (calculated by Kotochigova) became available and turned out to have values at large R and at $R=R_e$ or R_x very close to the empirical values. These *ab initio* functions resulted in improved fits to the data.

When modeling data over the full range from $v=0$ to the dissociation limit of the Na_2 $A\ ^1\Sigma_u^+$ state, coupled-channel methods together with accurate spin-orbit functions provide a unified approach to both the perturbation crossings at low v and the fine structure splitting near the dissociation limit. By contrast, for the A and b states of Li_2,[36] perturbation crossing effects are much smaller (the Li $2\ ^2P$ fine structure splitting is 0.336 cm^{-1} as compared with 17.1963 cm^{-1} for Na $3\ ^2P$). Spin-orbit effects near the $2\ ^2S+2\ ^2P$ dissociation limit in Li_2 have been addressed rigorously by analytic diagonalization of the coupled potentials in, for example, Refs. 37 and 38.

TABLE I. Sources of the data used in the present work. The first number in parentheses after A or b denotes vibrational numbers, after the semicolon, the rotational quantum numbers. PW, present work; Abs. Spec., absorption spectroscopy; LS, laser spectroscopy; Mod. Pop. Spec., modulated population spectroscopy; LES, laser excitation specroscopy; Mod. Gain, modulated gain; Pol. Spec., polarization spectroscopy; AOTR, all-optical triple resonance; DR, double resonance; PFAOTR, perturbation-facilitated all-optical triple resonance; FT, Fourier transform; PFOODR, perturbation-facilitated optical-optical double resonance.

	Authors	Year	Reference	Levels obs'd	Technique
1.	Kusch and Hessel	1975	8	$A(0-10)$	Photographic Abs. Spec.
2.	Kaminsky *et al.*	1976	9 and 10	$A(14-43)$ (113 lines)	Mod. Pop. Spec.
3.	Atkinson *et al.*	1982	12 and 13	$b(17,21,25;\leqslant 40)$	Mol. Beam LES
4.	Shimizu and Shimizu	1983	14	$b(8-17;\leqslant 20)$	Mol. Beam LES
5.	Ahmad-Bitar and Al-Ayash	1984	44	$A(22,25;\leqslant 26)$	Mol. Beam LES
6.	Gerber and Möller	1985	45	$A(v=68;\leqslant 12;v=66-70;0)$	Mol. Beam 2-step LES
7.	Effantin *et al.* and Babaky	1985	15 and 16	$A(0-10;0-104)$	FT emission from (2) $^1\Sigma_g^+$
8.	Chawla and co-workers	1985	21 and 22	$A(62-105;10,14)$	Mod. Gain Spec.
9.	Li *et al.*	1987	46	$A(26,34),b(28,34)$	Pol. Spec.
10.	Katô *et al.*	1988	47	$A(8),b(14)$	Pol. Spec.
11.	Whang *et al.*	1992	18 and 19	$b(0-7,32-57;3-18)$	PFAOTR
12.	Wang	1991	48	$A(44,48;10-14)$	AOTR
13.	Ji	1995	49	24 $A-b$ "window levels"	PFOODR
14.	Tiemann *et al.*	1996	23	$A(88-185;\leqslant 21)$	Mod. Beam 2-step LES
15.	Krämer *et al.*	1997	50	$b(0;0-14)$	Mol. Beam LES
16.	Zalicki *et al.*	1993	20	$A(0-3;2-85);b(6-9)$	Mol. Beam LES
17.	Li	1990	PW	$A(0-2,5,12,17,22),b(17,21)$	PFOODR
18.	Li, Lyyra, and Ahmed	2006	PW	$A(0-43;$ even $J\leqslant 16)$	DR Pol. Spec.
19.	Ross	2006	PW	$A(0-31;0-125)$	FT Abs. Spec.
20.	Qi, Bai, Ahmed, and Lyyra	2006	PW	$A(0-50;0-125)$	Pol. Spec.

For the A and b states of K_2, the DVR/FGH (Refs. 27 and 29) method has been used. A recent report[39] of data on the $A\ ^1\Sigma_u^+$ state of K_2 up to the dissociation limit extends these earlier results. Among alkali heteronuclear diatomics, extensive studies of interactions between the $A\ ^1\Sigma^+$ and $b\ ^3\Pi$ states of NaK have been presented in Ref. 40. A study of the A and b states of RbCs (Ref. 41) used the DVR approach, while a recent study of the A and b states of NaRb (Ref. 42) used an "inverted 4 coupled-channel approach" with an analytical mapping procedure for the R variation.

The availability of data on the Na_2 A state from $v=0$ to the dissociation limit also allows us to extract information on exchange effects as well as on dispersion terms in the long-range potential. This aspect is discussed in Sec. III C.

Because the traditional Dunham Y_{ij} parameters will not be obtained here, and in any case because there are spin-orbit coupling terms, it is not possible to obtain accurate term values without actually diagonalizing the DVR matrix for each J value of interest. This computational approach is actually quite straightforward, but for convenience of the reader, in the EPAPS file,[43] we provide full data tables that contain all the experimental data, corresponding fitted values, parameters, and also calculated term values over a wider range of energy and J. The intent here is to create a "dynamic" database for these states of Na_2. The gaps in the data should be apparent. If additional data are obtained, they can be combined with the previous available data and used to update the fitted parameters and improve predictions for unobserved levels.

In outline, we first discuss the older and then the unpublished and new experimental data (Sec. II). Section III explains the terms in our DVR Hamiltonian, including short-range potentials, dispersion, exchange, and spin-orbit terms, and then presents fitted parameters and term value results. We conclude with comments on the DVR Hamiltonian matrix approach.

II. THE EXPERIMENTAL DATA

The new and old sources for the data used in this study are summarized in Table I. Below, we give additional details about the older published data and more extensive information about the new data. A representation of all the data is shown in Fig. 1. Dots are plotted for the state that is calculated to have the largest component in the DVR eigenvalue calculated for each experimental term value. Clearly, the preponderance of the data is for the $A\ ^1\Sigma_u^+$ state, and there are gaps in the data for the $b\ ^3\Pi_u$ state. By way of orientation, potentials for the states of interest are shown in Fig. 2.

We have chosen to use the minimum of the X state as the zero of energy. The fitting procedures here use term values rather than combination differences except as noted in Sec. III B.

When combining data from many sources into a global fit, one key question is the relative weight given each data set. Nominally, the weight for each data point is equal to $1/\sigma^2$, where σ is the estimated uncertainty. Where possible, we have used the published experimental uncertainties. However, comparisons of observations of the same term values from different data sets and our own experience in calibrating spectra with iodine lines have in several cases led to upward adjustment of these uncertainties.

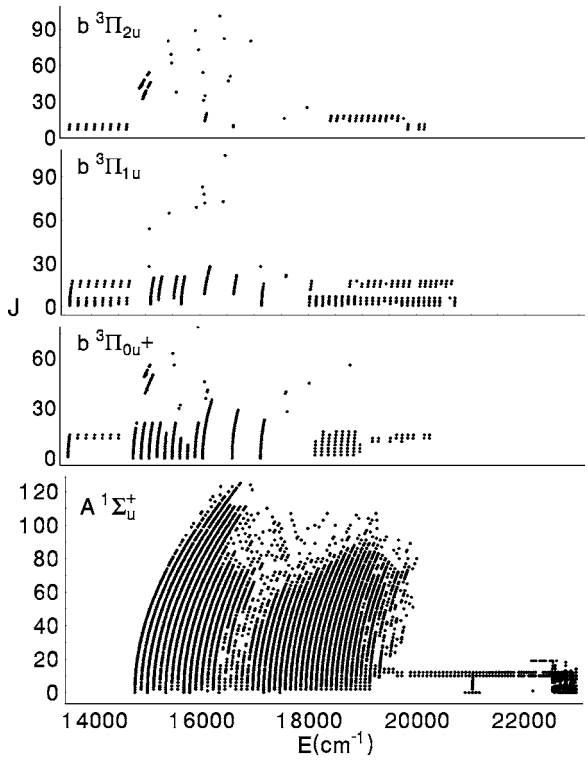

FIG. 1. Summary of the data used in this study. The observed term values are sorted according to the largest component in the calculated eigenvector.

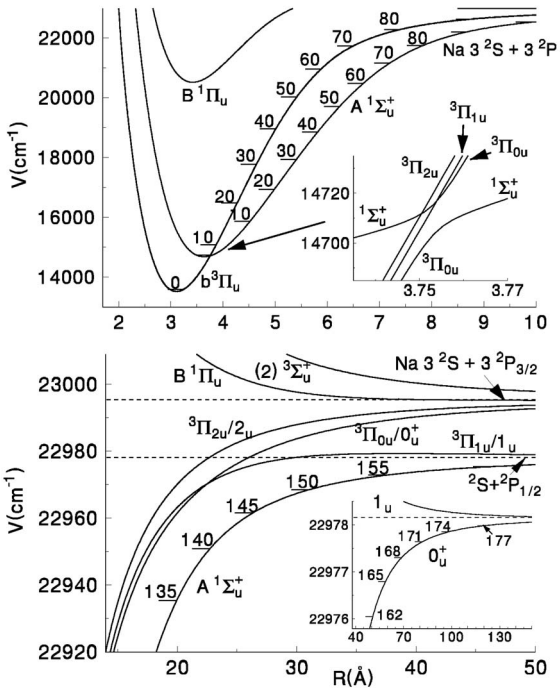

FIG. 2. Adiabatic potentials for Na_2 *ungerade* states in the energy region of this study, obtained by diagonalizing the DVR matrix for $J=|\Omega|$, for each value of R. Vibrational quantum numbers are shown for the A and b states. The top plot shows the lower levels, with an inset showing the avoided crossing region. The bottom plot, also with an inset, shows levels and turning points closer to the dissociation limit. Eigenvalue calculations, however, used diabatic potentials and spin-orbit coupling functions.

A. Data previously published

Kusch and Hessel[8] used a 9.3 m concave grating spectrograph to study the Na_2 $A \leftarrow X$ band system. Parameters for the A state were extracted by ignoring perturbed levels. Perturbation shifts of $v=0$ and 1 rotational levels of the A state are displayed in a plot in Ref. 8. We have been told that Kusch discarded the raw spectral data shortly before he died. From the Y_{ij} parameters and the plotted shifts, we reconstructed term values for A state $v=0$ and 1 levels and used these estimates at an early stage of this study.

One of the prominent early achievements of laser spectroscopy was the thesis[9] of Kaminsky with Schawlow. Modulated population spectroscopy[10] was used to separate individual absorption lines from the dense spectral background. 113 transitions are listed in Ref. 9 with A state quantum numbers ranging from $v=14$ to 43 and J values primarily 12, 14, 27, 29, 42, and 44. The quoted uncertainties of 0.03–0.30 cm^{-1} are relatively large, so the data were used only in the early phases of this study.

Direct observation of spin-forbidden transitions $b\ ^3\Pi_u \leftarrow X\ ^1\Sigma_g^+$ was made possible by observing laser-induced fluorescence from a molecular beam.[13] In the thesis of Atkinson,[12] data for the b-X (17,0), (21,0), and (25,0) bands, each with all three Ω components, are given for J values from 0 to 40.

A wider range of b state vibrational levels, from $v=8$ to 17 (but with $J \leqslant 20$), was observed, also by molecular beam laser-induced fluorescence, by Shimizu and Shimizu.[14] Although the quoted calibration uncertainty is 0.0015 cm^{-1}, comparisons of data on the same vibronic levels in the previous data set exhibited differences as large as 0.008 cm^{-1}. Therefore, each set was given a standard deviation σ of 0.005 cm^{-1}.

Ahmad-Bitar and Al-Ayash[44] reported observations of ten $A \leftarrow X$ bands by laser absorption of a supersonic molecular beam, with 40 MHz linewidth. Unfortunately, line positions were given only for the (25,3) and (22,1) bands.

High vibrational levels ($v=66$–70) of the A state were observed by Gerber and Möller using two-step excitation in separate interaction regions of a molecular beam.[45] From the first region, excited A state levels decay to $v''=31$ of the X state, which were reexcited. Here also, the published line measurements the (68,31) band are a regrettably small fraction of the total.

We have also been able to use a more extensive set of spectral line data from the work of Effantin *et al.*[15] The A state was observed in emission from the (2) $^1\Sigma_g^+$ state, which was populated by collisional transfer from the $B\ ^1\Pi_u$ state, which in turn was excited by several Ar^+ laser lines. The data cover the range $0 \leqslant v \leqslant 10$ of the A state, with $J \leqslant 104$. We transcribed more than 5000 handwritten line measurements into electronic files. By comparison with term values obtained from $A \leftarrow X$ transitions, this data set yields apparent shifts of 0.01–0.05 cm^{-1}, possibly due to collisional transfer from the level originally excited to another level from which fluorescence was observed.

In order to access higher levels of the A state, Chawla and co-workers[21,22] used modulated gain spectroscopy. This involved excitation of $v=7$ or 26 of the A state by a pump

laser, and then decay in a resonant cavity to sparsely occupied $v=19$ or 39, respectively, of the X state, thereby producing an "optically pumped laser (OPL)." Transitions to $v=62-105$ levels of the A state were detected by their effect on the gain of the OPL. P/R doublets with $J''=11$ were measured to an accuracy of 0.006 cm^{-1}.

Li *et al.*[46] used pump-probe techniques to selectively observe certain $A \leftarrow X$ transitions. In particular, they studied perturbations between $A(v=26)$ and $b(v=28)$ and between $A(v=34)$ and $b(v=34)$. Although a heat pipe oven was used, the geometry of the pump-probe technique reduced the linewidth to a residual linewidth of 25 MHz.

At about the same time, Katô *et al.*[47] used Doppler free polarization spectroscopy to study the perturbative interactions between $A(v=8)$ and $b(v=14)$. Resolved hyperfine structure was also reported in this work.

Whang *et al.*[18,19] used perturbation-facilitated all-optical triple resonance (PFAOTR) to observe a large number of levels of the b state. A level of the A state mixed with the triplet b was the first excitation step, followed by excitation to a level of the $2\ ^3\Pi_g$ state, and then stimulated decay to b state levels. Various rotational levels $3 \leqslant J \leqslant 18$ with $v=0-7$ and 32–57 of the b state were observed by monitoring fluorescence of the $2\ ^3\Pi_g$ state. The cumulative measurement uncertainty from these multiple steps was estimated to be 0.01 cm^{-1}.

Another AOTR scheme was used by Wang[48] to excite moderately high levels of the A state. Low levels of the A state were first excited from the X state, followed by stimulated decay to high levels of the X state, and reexcitation to higher levels of the A state. Levels with $J=10$, 12, or 14 for $v=44-48$ and 55–61 were observed, with uncertainties estimated to be 0.02 cm^{-1}.[48]

As part of a thesis on long-range potentials in K_2 and Na_2, Ji[49] used singlet-triplet $A \sim b$ levels as window states to access higher triplet states. This thesis lists 24 such mixed levels that were observed in the course of a study of the Na_2 (1) $^3\Delta_g$ state.

Tiemann *et al.*[23] were able to excite levels of the A state up to the dissociation limit by Franck-Condon pumping from $v=0$ to $v=27$ or 31 of the X state via $v=13$ of the A state, followed by excitation with a second laser to $v=88-185$ of the A state. Because of a high degree of collimation of the molecular beam, the residual Doppler width was only 5 MHz. Experimental uncertainties mostly vary between 0.0003 and 0.030 cm^{-1}, but in a few cases from overview spectra recorded with a multimode laser, they amount to 0.15 cm^{-1}.

Krämer *et al.*[50] used a beam of Na_2 molecules to directly excite the intercombination transition from $X(v=0)$ to $b(v=0)$. $\Omega=0$ and 1 components of the b state were observed up to $J=14$, with a calibration accuracy of 0.015 cm^{-1}.

B. Unpublished data

Laser spectroscopy with a molecular beam. Zalicki *et al.*[20] in 1993 at Laboratoire de Spectroscopie Hertzienne de l'ENS and at the Université Pierre Marie Curie, Paris, used a supersonic beam of Na_2 molecules and a ring dye laser to excite $v=0-3$ of the A state to study perturbations with $v=6-9$ of the b state. The spectral linewidth was typically greater than 40 MHz (the residual Doppler width), as many transitions were power broadened to increase the detection sensitivity for transitions that were predominantly $b \leftarrow X$ character. 392 term values, $2 \leqslant J \leqslant 85$, from these observations are included in the present data set. Calibration was with a wave-meter and iodine reference lines. For levels with appreciable triplet character, the hyperfine structure was well resolved. For this study, the hyperfine center of gravity was taken as the effective line center. The rotational populations of ground state levels were studied in a separate work.[51]

Perturbation-facilitated optical-optical double resonance spectroscopy. This technique was used especially to measure mixed singlet-triplet states for use as window states to excite higher triplet levels. 117 levels were excited over a wide range of energies by one of us [Li; data obtained at MIT (1982–1984), University of Iowa (1987–1989), and Temple University (1993–2001)].

Optical-optical double resonance polarization spectroscopy. This technique was used earlier in this study (at the University of Iowa in 1990, by Li and Lyyra, with calibrations verified later by Ahmed) to obtain data on 544 A state levels up to $v=44$, even with J values $\leqslant 16$. The "V-type" polarization scheme has been described in Refs. 52 and 53 and differs from the technique described below in that the pump laser excited a different upper state than the probe laser. For other examples of this technique as applied to higher electronic states of Na_2, see Refs. 54 and 55.

Absorption spectroscopy. A Doppler-limited absorption spectrum of Na_2 was recorded (by Ross, in Lyon) on a Fourier transform spectrometer at an instrumental resolution of 0.02 cm^{-1}, in part to replace the lost original data of Ref. 8. Na_2 molecules were formed in a short (20 cm) heat pipe oven, operated at 480 °C with argon as a buffer gas. Measured widths (full width at half maximum) of isolated lines were Doppler limited (0.05 cm^{-1} at 17 200 cm^{-1}). Instrumental calibration was checked by recording the absorption spectrum of I_2 with the same optical alignment. Nearly 10 000 lines were measured over the range 13 300–17 200 cm^{-1}. At the high energy end, line assignments were complicated by extensive overlapping due to the Doppler linewidths. Polarization spectroscopy eventually provided data at higher resolution, so the absorption spectra data were not actually included in the final fit.

Polarization spectroscopy. Extensive new measurements of Na_2 $A \leftarrow X$ transitions have been performed (by Qi, Lyyra, and Bai) at Temple University using the technique of polarization spectroscopy.[24] This technique was first used to observe hyperfine structure in the hydrogen atom Balmer-β transition,[56] and more recently, it has been used in molecular spectroscopy studies.[36,52,57] The basic principles are clearly discussed in Refs. 52 and 58 and will be reviewed here very briefly.

For polarization spectroscopy, a linearly polarized single mode tunable laser beam is split into a weak probe beam and a pump beam (see Fig. 3). The stronger pump beam passes through a $\lambda/4$ wave plate and becomes a circular polarized beam (either left handed or right handed). The probe beam

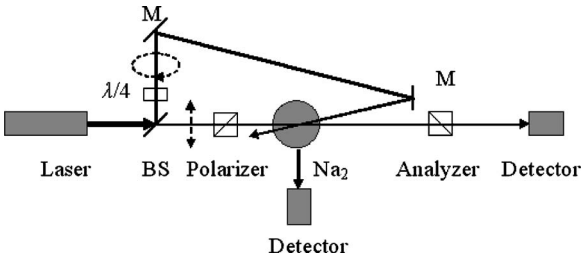

FIG. 3. A schematic of the experimental setup for polarization spectroscopy. Lateral detection of the total fluorescence records a Doppler-limited laser excitation spectrum.

passes through a polarizer, the molecular sample, and an analyzer, a polarizer crossed with the first one. The linearly polarized probe beam and the pump beam counter-propagate. The sample is isotropic without the pump beam and the detector only receives a very small residual signal from imperfectly crossed polarizers or some birefringence of the cell windows.

The pump is absorbed by the molecular sample when the optical frequency is tuned to a molecular transition, which we write as $(J',M') \leftarrow (J'',M'')$, where M denotes the magnetic quantum number referred to an axis along the direction of beam propagation. In zero external field, the M components are degenerate and equally populated. However, the transition amplitudes for the pump beam vary with M, and thus certain magnetic sublevels are partially depleted by the pump beam. For this reason, the originally isotropic molecular sample becomes anisotropic in the presence of the pump beam. When the probe beam passes through the anisotropic molecular sample, each circular component will experience a different phase shift and also a differential absorption. From both effects, there will be a signal through the crossed polarizers, provided that the pump and probe beams interact with the same molecules. Since they are traveling in opposite directions, this implies that the affected molecules will be those with negligible Doppler shift; hence, this makes sub-Doppler width spectroscopy possible.

As discussed in Refs. 24, 52, and 58, the resultant signal has Lorentzian and dispersion components. The orientation of the analyzer prism can be adjusted to null out the dispersion term and maximize the Lorentzian term. Figure 4 shows part of a typical scan together with the I_2 laser excitation spectroscopy (LES) signal, the Vernier étalon (VET) channel, which is used to monitor mode hops during the laser scans, and a LES signal also from Na_2, exhibiting a Doppler linewidth. Mode hops appear as discontinuities in the VET scan. Each 1 cm^{-1} segment consists of three 10 GHz continuous scans and the joints of these segments introduce some uncertainty into the calibration. Iodine lines within each 10 GHz segment are used for calibration of that segment. When no calibration lines appeared in a 10 GHz segment, interpolation between adjacent segments was required. The calibration procedure was based on the Doppler-limited iodine atlas,[59] with corrections from Ref. 60 and later by Ref. 61. Overall, the mean calibration uncertainty was estimated to be 0.005 cm^{-1}. The heat pipe oven temperature for these experiments was 570 K.

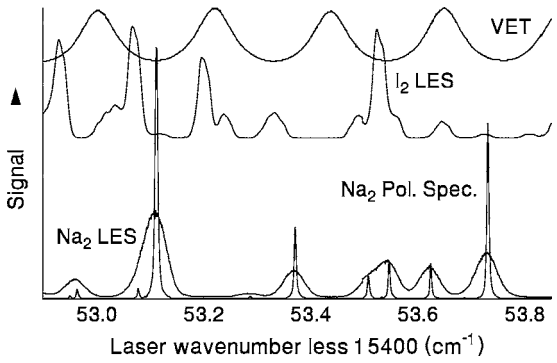

FIG. 4. A typical region of the polarization spectrum showing (top) the vernier etalon signal (VET) signal used to check that the laser scans continuously, (middle) the I_2 LES signal for calibration, (bottom) the Doppler-limited Na_2 LES signal, and the Na_2 polarization spectroscopy signal, which exhibits a sub-Doppler width.

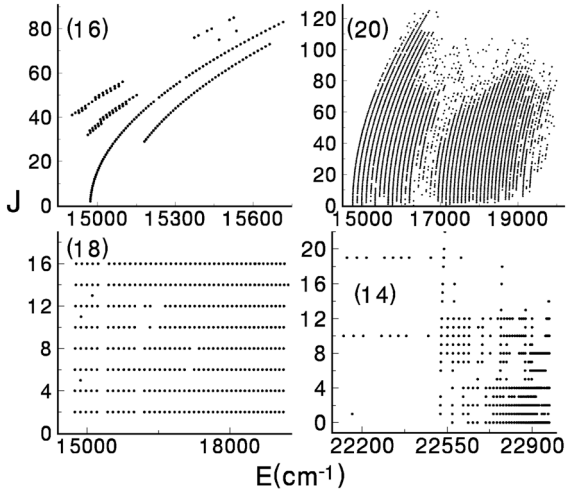

FIG. 5. The range of the data for the Na_2 A and b states from several of the individual data sets. The numbers in parentheses refer to the data source numbers listed in the first column of Table I.

Figure 5 shows the range in energy and rotational quantum number for four of the unpublished data sets listed above. In other cases, the range is clear from the discussion or the publication.

In each case where term values are calculated from experimental lines, the Na_2 X state Y_{ij} parameters of Ref. 62 (data set II) (hereafter referred to as KHII) have been used. A value of $Y_{00}=-0.031\,77$ cm^{-1} for the X state is obtained from these Y_{ij} values. The $G(v)$ values given by Ref. 63, and from combination differences obtained from the lines measured by Ref. 24, agree with the KHII values within 0.006 cm^{-1}. However, recent measurements cited in Refs. 23 and 64 give energies of X state levels $J=0$, $v=27$ and 31 that are smaller than predictions from KHII by 0.0197(44) and 0.0170(37) cm^{-1}, respectively. The term values from Refs. 21 and 45 have been adjusted accordingly. In general, one can say that the accuracy of A and b state level energies presently is tied to both the wavelength calibration accuracy and the accuracy of the energies of the X state. Further improvement might require an alternative calibration technique, such as frequency combs.

The dissociation limit D_0 of the X state to the free atom hyperfine center of gravity (hfs cog) has been accurately determined by Ref. 64 to be $D_0=5942.6880(49)$ cm^{-1}. In this work, energies are referenced to the minimum of the X state, which lies 79.3426 cm^{-1} below $v=0$, as obtained from the Y_{ij} parameters of KHII and Y_{00} given above. From Ref. 65, the transition energy from hfs cog energies of a $3\,^2S$ atom to a $3\,^2P_{1/2}$ atom is 16 956.170 27(4) cm^{-1}. From the $3\,^2P_{1/2}$ cog to the cog of the $3\,^3P$ state, it is 11.4639 cm^{-1} [$(2/3)\Delta_{\text{atom}}=17.1959$ cm^{-1}]. Since spin-orbit structure is considered here, the relevant quantity is thus a dissociation limit of 22989.6648 cm^{-1}. Technically, the threshold for free $^2S(F=1)+{}^2P_{1/2}(F=1)$ atoms lies at a limit of 22 978.1599 cm^{-1}. However, we have found that the experimental data extrapolate essentially to the hfs cog, which has a limiting value of 22 978.2009 cm^{-1} and is consistent with the $3\,^2S+3\,^2P$ fine structure cog of 22 989.6648 cm^{-1} as given above. Although the experimental data from Ref. 23 extend to $v=185$, only data to 22 978.05 cm^{-1} (slightly above $v=177$ as shown in Fig. 2) were included in the analysis to avoid hyperfine structure effects, which are not included in the present model, but were of primary concern in Ref. 23.

For absorption spectroscopy or single-photon polarization spectroscopy, the range of accessible upper state levels is limited by the transition strengths, which are determined by the vibrational overlap factor including the A-X electronic transition dipole moment $\langle A(v')|\mu(AX)|X(v'')\rangle$, and the Boltzmann thermal factor for the X state level. The electronic transition dipole moment function is obtained from *ab initio* psuedopotential calculations and confirmed by experiments in Ref. 66. Results are plotted in Fig. 6. We have calculated the line strengths using a Boltzmann factor, $\exp[-E(v'',J'')/k_BT]$, and the A-X electronic transition dipole moment function, $\langle A(v')|\mu(AX)|X(v'')\rangle$, obtained from pseudopotential *ab initio* calculations and confirmed by experiments by Ref. 66. Results are plotted in Fig. 6.

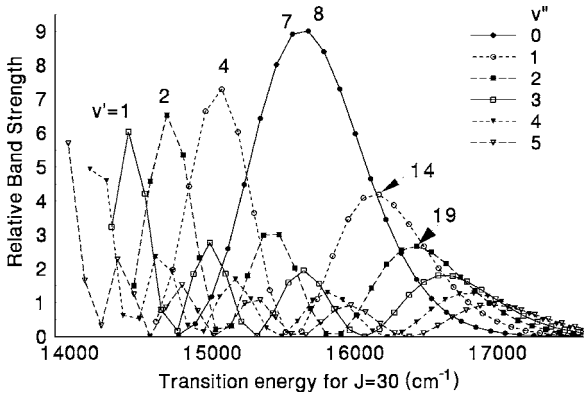

FIG. 6. This plot shows relative band intensities, calculated from the product of the vibrational overlap, $|\langle A(v')|\mu(AX)|X(v'')\rangle|^2$, including the $A\leftarrow X$ transition moment from Ref. 66, times the Boltzmann factor, $\exp[-E(v'',J'')/kT]$. Here, $T=600$ K, $J''=30$.

III. FITTED POTENTIALS AND SPIN-ORBIT FUNCTIONS

A. Molecular Hamiltonian

This study of interactions between the $A\,^1\Sigma_u^+$ and $b\,^3\Pi_u$ states of Na_2 is limited to levels of parity $(-1)^J$, e symmetry, by selection rules. We will not address hyperfine structure effects and therefore $\Delta J=1$ hfs couplings with f symmetry levels, parity $-(-1)^J$, and $\Delta J=0$ hfs couplings between g and u states will not be not considered.

The molecular Hamiltonian[67] includes elements for (radial) kinetic energy H_K, nuclear rotation H_{rot}, and potential energy including spin-orbit effects H_V:

$$H(R)=H_K+H_V(R)+H_{\text{rot}}(R), \tag{1}$$

where R is the internuclear distance. Spin-orbit functions are discussed in Sec. III D. Since the present data extend to very near the dissociation limit, we use forms for the rotational energies that are transformed to case a from the case e expressions, as in Ref. 68. Hence, $G(v)$ values may differ from other conventions. For this reason, in presentations below, we will refer to our vibrational energies with the notation $\tilde{G}(v)$, which translates to the usual convention for $^1\Sigma_u^+$ states as $G(v)=\tilde{G}(v)+2B_e$ (see, for example, Table IV). For e symmetry levels, the nonzero matrix elements of $H_V(R)+H_{\text{rot}}(R)$ are

$$\begin{aligned}
&\langle {}^1\Sigma^+|H|{}^1\Sigma^+\rangle = V({}^1\Sigma^+)+(x+2)B,\\
&\langle {}^3\Pi_\Omega|H|{}^3\Pi_\Omega\rangle = V({}^3\Pi)+(\Omega-1)\Delta_{\text{d}}+(x+2\epsilon)B,\\
&\langle {}^1\Sigma^+|H|{}^3\Pi_{0^+}\rangle = -\Delta_{\text{od}},\\
&\langle {}^3\Pi_0|H|{}^3\Pi_1\rangle = -\sqrt{2x}B,\\
&\langle {}^3\Pi_1|H|{}^3\Pi_2\rangle = -\sqrt{2(x-2)}B,
\end{aligned} \tag{2}$$

where $x=J(J+1)$, $\epsilon=1$ (for $\Omega=0$ and 1) and -1 (for $\Omega=2$), and $H^\dagger=H$. In the above, $V(^1\Sigma_u^+)$, $V(^3\Pi_u)$, Δ_{d}, Δ_{od}, and $B=B(R)=\hbar^2/2\mu R^2(1/100hc)$ are functions of R (μ is the reduced mass). (Here μ, R, $\hbar$, and c are in SI units, and all V, Δ, and B quantities are in cm^{-1}. The factor $1/100hc$ converts from SI units to conventional spectroscopic cm^{-1}.) Δ_{d} and Δ_{od} are diagonal and off-diagonal spin-orbit functions, respectively.

For test purposes, we also preformed six-channel calculations using additional Hamiltonian elements for the $B(1)\,^1\Pi_u$ and $(2)\,^3\Sigma_u$ state plus coupling elements between these states and those represented in Eq. (2). Such elements are given in Refs. 67 and 68. Since the R dependence of the additional spin-orbit functions and L-uncoupling functions is not known, we took these functions to be constant with the value appropriate for the asymptotic limit. These additional elements are needed to produce exact convergence to the $3\,^2S+3\,^2P$ center-of-gravity limit without spin-orbit functions, or to the $P_{1/2}$ and $P_{3/2}$ limits with spin-orbit functions, as shown in Fig. 2, for which the potentials are obtained by diagonalization of the DVR matrix at each R value (for $J=|\Omega|$). Although the Hamiltonian matrix elements in Eq. (2) by themselves do not converge to the correct limit, we found that up to $v=177$ of the A state, the difference in eigenenergies between four- and six-channel calculations was no more

than 3 MHz. Hence, given the present limited objectives, four-channel calculations are deemed sufficient.

The DVR Hamiltonian matrix has a dimension equal to the number of R mesh points, i, times the number of channels ($^1\Sigma_u^+$, $^3\Pi_{0u}$, etc.), j ($\leqslant 4$ in the present approximation). The elements in Eq. (2) are diagonal in i but may be off-diagonal in j. Since all mesh points are used in calculating d^2/dR^2,[31] the kinetic energy (a full matrix over i) is obtained as accurately as possible. As in Ref. 35, scaling is used to make the mesh points more dense where the momentum can be greatest, namely, for R values near minima of the potentials. The eigenfunctions obtained by diagonalizing the DVR matrix give the wave function components in each channel. The eigenvalues include effects of mixing between different channels, including the continua. Hence, this approach is a powerful alternative to calculating vibronic coupling elements with wave functions obtained by the Numerov method, but does require diagonalization of a fairly large matrix for each J value. Applying the DVR method, experimental term values are used to fit potential and spin-orbit function parameters. Accurate term values for perturbed levels can be obtained only by solving the DVR eigenvalue problem for the coupled states, or from tables, as given in the EPAPS files.[43]

B. The fitting process

As stated above, in this study there were several stages in fitting the data to potential and spin-orbit parameters as more detailed data were obtained. At each stage, intensities were estimated from calculated A-X Franck-Condon factors, rotational line strengths, and the X state Boltzmann factor for the experimental temperatures. The new polarization spectroscopy lines were matched with calculated line positions to successively smaller tolerances, ultimately 0.02 cm^{-1}. All term values calculated from these lines (by adding ground state energies) were given a σ (uncertainty) of 0.005 cm^{-1}. Values for σ varied between 0.002 and 0.02 cm^{-1} for the other data sets.

We used 24(12) nonzero short-range potential parameters for the $A(b)$ state, 4 long-range potential parameters for each, and spin-orbit parameters as discussed below. Normally, not more than 15 parameters were varied simultaneously, but from iteration to iteration, the parameter set was traversed several times. For levels up to 10 cm^{-1} below the dissociation limit, it was sufficient to carry the DVR mesh points in R out to 40 Å, with 320 mesh points in R, giving a 1280×1280 DVR Hamiltonian matrix for four-channel calculations for each $J\geqslant 2$. For levels closer to the dissociation limit, as many as 1500 mesh points out to $R=150$ Å were used, but these cases involved only J values $\leqslant 22$.

Some of the data from Ref. 23 with the smallest experimental uncertainties, including data close to the $3S+3P_{1/2}$ dissociation limit, were in the form of difference frequencies. Four-channel calculations using our fitted parameter set reproduced these difference frequencies to within 20 MHz, except for a few outliers and also data from levels within 1 cm^{-1} of the $P_{1/2}$ dissociation limit, where evident hyperfine

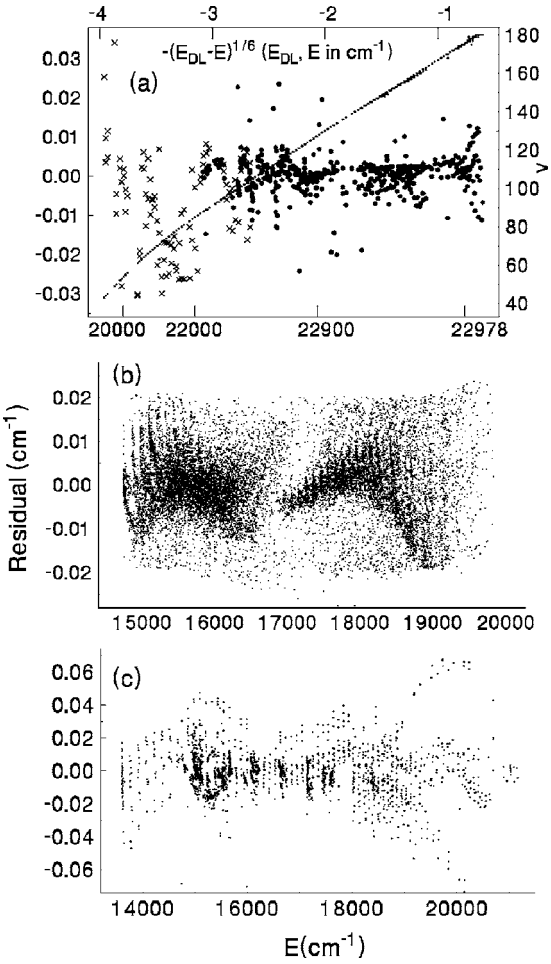

FIG. 7. Residuals from (a) the data from Refs. 23 (dots) and 21 (crosses), (b) the new polarization spectroscopy data, and (c) all other data sets included in the fit. The energy in (a) is scaled as $(E_{DL}-E)^{1/6}$ to expand the region near the dissociation limit, $E_{DL}=22\,978.2009$ cm^{-1}, so as to show systematic effects due to hyperfine structure above $E=22\,978$ cm^{-1}. Vibrational quantum numbers (smaller dots in a nearly straight line) are plotted with reference to the right axis. Data for (b) were selected to be within 0.02 cm^{-1} of the energy calculated from the fitted parameters.

effects increased the residuals to as much as 150 MHz. A detailed study of the regime very near the dissociation limit is beyond the scope of the present work.

The overall variance of the fit of A/b data within the present data set to potential and spin-orbit parameters was 2.85, after many iterations. To indicate the quality of the fit, we plot in Fig. 7(a) the residuals from the two data sets at the highest energy, in Fig. 7(b) the residuals from the new polarization spectroscopy data, and in Fig. 7(c) the residuals for the other data sets. The final rms residual for the former was 0.0080 cm^{-1} (240 MHz). Combination differences for the X state from this data set agreed with $E(v,J)$ values calculated from the Y_{ij} parameters of KHII (Ref. 8) to a rms residual of 0.006 cm^{-1}.

From the residuals plotted in Fig. 7, it does appear that couplings with states outside the Hamiltonian basis may produce small J-dependent shifts. The most likely culprits are the $B\ ^1\Pi_u$ state coupling with the $A\ ^1\Sigma_u^+$ state and the $a\ ^3\Sigma_u^+$ state coupling with the $b\ ^3\Pi_u$ levels. We did attempt to introduce $A\sim B$ L-uncoupling terms into a larger Hamiltonian matrix, but the results were not decisive, and in any case, the

R dependence of such elements is not known. Therefore, all results quoted here are from the four-channel Hamiltonian matrix, as stated above.

C. The potential functions

The Born-Oppenheimer potential functions are divided into short-range and long-range regions. The long-range potential for the A state is composed of the exchange potential and dispersion terms: $V_{LR}(R)=V_{exch}+V_{disp}$. Typically, the transition point R_T is chosen to be comparable to the Le Roy radius,[69] R_{LR}, which indicates approximately the R value at which the atomic wave function overlap becomes negligible, and the expansion in inverse powers of R becomes valid. The original estimate[69] from atomic radii, $R_{LR}=2[\langle r^2\rangle_A^{1/2}+\langle r^2\rangle_B^{1/2}]$, was found to be inadequate for excited states, and an m-dependent expression was introduced in Ref. 70: $R_{LR\text{-}m}=2\sqrt{3}[\langle nlm|z^2|nlm\rangle_A^{1/2}+\langle n'l'm'|z^2|n'l'm'\rangle_B^{1/2}]$, to represent the orientation of the atomic orbitals. Here, n and n' are principal quantum numbers, l and l' are the atomic electronic orbital angular momenta, and m and m' are the components of l and l' along the internuclear axis for the outermost electrons. For Na_2 $3s_\sigma+3p_\sigma$ and $3s_\sigma+3p_\pi$, the values of $R_{LR\text{-}m}$ from Ref. 70 are 13.4 and 9.7 Å, respectively. There are no experimental b state term values above 20 700 cm^{-1}, corresponding to an outer turning point of 5.75 Å, so there is no direct information on the long-range part of the potential for the b state. However, as the available data on the A state extends to nearly the dissociation limit, it is possible to extract information on both the long-range coefficients and the exchange potential for this state.

For the short-range region, $R\leqslant R_T$, we use the analytic expression adopted by the Hannover group,[27,28]

$$V_{SR}(R)=\sum_{i=0}^{I} a_i\left(\frac{R-R_M}{R+bR_M}\right)^i. \tag{3}$$

In this work, we typically set $a_1=0$, so that $R_M=R_e$, the R value at the potential minimum, and thus $a_0=T_e$. The parameter b was adjusted to achieve an optimum fit with a minimum number of parameters. The advantage of this parametrization as compared with the traditional Dunham/RKR approach is that the semiclassical approximation does not enter, and the divergence at large R is less of a problem, since $V_{SR}(R\to\infty)=\Sigma_i a_i$ is finite (though extremely large).

Note that if $a_1=0$ in Eq. (3), then it follows that

$$\frac{\partial^2 V}{\partial R^2}(R=R_e)=\frac{2a_2}{R_e^2(1+b)^2};$$

$$\Rightarrow \omega_e=\frac{1}{10\pi(1+b)R_e}\left(\frac{ha_2}{2\mu c}\right)^{1/2}, \tag{4}$$

where μ is the reduced mass. μ, h, c, and R_e are in SI units, while a_2 and ω_e are in cm^{-1}. The potential parameters a_i for the $A\ ^1\Sigma_u^+$ and $b\ ^3\Pi_u$ states are listed in Table II. Fitted values for T_e, ω_e, and R_e are given in Table III. As stated above, for purposes of comparisons in Table III, we present our results in the form $T_e=\tilde{T}_e+2B_e$ for the A state and $T_e=\tilde{T}_e+B_e$ for the b state. Term values calculated with the A state parameters of Ref. 8 give $v=0$ term values about 0.06 cm^{-1} higher than observed in the present work. Results from Refs. 20 and 24 and from absorption spectroscopy in Lyon agree to within less than 0.01 cm^{-1}, suggesting a 0.06 cm^{-1} calibration error in the earlier work of Ref. 8. The remaining difference in the A state values for T_e is due to perturbation shifts that were not analyzed in Ref. 8. In Table III, the uncertainties for T_e and ω_e are determined primarily by wavelength calibration uncertainties. Note that the uncertainties for R_e values reflect a range of rotational energies spanning 500–1000 cm^{-1}, and that centrifugal distortion effects are determined by the potential function rather than by additional parameters. However, L-uncoupling interactions with states outside the four-channel Hamiltonian matrix and also possible sensitivity to the form of the potential are not included in the estimates of the uncertainty of the R_e values.

TABLE II. Fitted parameters for the V_{SR} potential function, for the A and b states. $T_e=a_0$ and R_e are given in the following table. $a_1=0$. The a_i are in cm^{-1}, while b is dimensionless. Numbers in square brackets denote the power of 10. For the A state, $R\leqslant 2.357$ Å, the form $V=A/R^4+C$ applies, with values given below.

	A state	b state
b	1.692 142 646	0.230
a_2	2.252 672 639 84[5]	5.928 917 446 45[4]
a_3	−6.999 292 760 99[5]	−2.244 248 711 459[3]
a_4	9.633 810 729 92[5]	−6.676 242 575 792[4]
a_5	9.050 944 761 15[5]	−9.877 399 975 864[5]
a_6	−1.353 816 744 09[7]	1.990 153 164 054[5]
a_7	1.968 679 893 00[7]	5.521 114 946 502[5]
a_8	1.778 001 698 55[8]	−2.169 520 362 189[6]
a_9	−1.245 607 952 89[9]	−2.884 323 344 369[6]
a_{10}	2.193 078 450 59[9]	8.119 353 310 882[6]
a_{11}	2.802 520 057 56[10]	4.259 151 884 120[5]
a_{12}	−2.397 623 078 49[11]	
a_{13}	6.090 618 458 01[11]	A state, $R\leqslant 2.357$ Å:
a_{14}	6.476 255 150 53[11]	$V(R)=A/R^4+C$;
a_{15}	−4.752 613 018 90[12]	$A=7.187\,53[5]$ cm^{-1} Å^4
a_{16}	−2.489 570 504 02[12]	$C=2.457\,835\,9[3]$ cm^{-1}
a_{17}	4.002 905 840 06[13]	
a_{18}	−4.334 056 442 24[13]	
a_{19}	−1.837 113 429 17[14]	
a_{20}	8.301 971 726 55[14]	
a_{21}	−1.704 450 623 24[15]	
a_{22}	1.883 672 875 43[15]	
a_{23}	−8.737 759 108 58[14]	

The exchange interaction for a $^1\Sigma_u^+$ state from $3s+3p$ atoms, as given by Bouty *et al.*[71] (see also Refs. 72 and 73), is

$$V_{exch}=q[I(310,300|310,300)+I(310,300|300,310)], \tag{5}$$

where q is an amplitude factor that was adjusted in the fitting process. The two integrals, $I(n_1,l_1,m_1,n_1',l_1',m_1'|n_2,l_2,m_2,n_2',l_2',m_2')$, represent exchange with and without excitation transfer.[71] Each includes a factor $(A_{3s}A_{3p})^2$ which is uncertain to some degree, so it is considered appropriate to adjust q [the quotient, optimized value/*ab initio* value, of $(A_{3s}A_{3p})^2$] in the fitting process.[74]

The dispersion terms in V_{LR} are given by

TABLE III. Potential parameters. T_e and ω_e are in cm^{-1}, R_e in Å, and the C_n parameters are in units cm^{-1} $Å^n$. The parameters used in the exchange potential $A_{3s}A_{3p}$ are dimensionless. PW=present work. Numbers in square brackets after a series of digits denote the power of 10, while parentheses denote uncertainty limits, which for the present work are discussed in the text.

Parameter	Ref.	*A* state	*b* state
T_e	8	14 680.541	
	15		13 523.19(275)
	18		13 520.946(9)
	PW	14 680.396 4(50)	13 520.897(8)
ω_e	8	117.316 43	
	15		153.84(62)
	18		154.209(4)
	PW	117.3881(30)[a]	154.236(12)[a]
R_e	8	3.634 78	
	15		3.115 1(84)
	18		3.106 67(41)
	PW	3.637 507(7)	3.108 645(14)
$A_{3s}A_{3p}$	71	0.122 4	
	PW	0.186 6(20)	
C_3	81	4.069[5]	2.035[5]
	80	4.212[5]	2.106[5]
	82	3.987[5]	1.994[5]
	23	4.047(13)[5]	
	83	4.0402(52)[5]	
	PW	4.0508(30)[5]	2.025[5][b]
C_6	81	2.007[7]	1.294[7]
	80	1.997[7]	1.286[7]
	82	1.921[5]	1.270[7]
	PW	1.8898(800)[5]	1.270[7][c]
C_8	81	9.143[8]	1.111[8]
	80	9.691[8]	7.498[7]
	82	9.481[8]	1.155[8]
	PW	1.543 7(1000)[9]	1.155[8][c]

[a]Results obtained from Eq. (4).
[b]The *b* state C_3 value is fixed at one-half the *A* state C_3 value.
[c]Fixed at the results of Ref. 82.

$$V_{\rm disp} = -f^{\Sigma,\Pi}\frac{C_3^{\Sigma,\Pi}}{R^3} - \frac{C_6^{\Sigma,\Pi}}{R^6} - \frac{C_8^{\Sigma,\Pi}}{R^8}, \tag{6}$$

where the $f^{\Sigma,\Pi}$ are retardation corrections that are marginally significant here: $f^{\Sigma}=\cos(x)+x\sin(x)$, $f^{\Pi}=f^{\Sigma}-x^2\cos(x)$, where $x=2\pi R/\lambda$, with λ the transition wavelength. For the *A* state, the retardation correction $(f^{\Sigma}-1)C_3/R^3$ reaches 0.040 cm^{-1} at 6 Å, decreasing for larger *R* values. The $1/R$ dependence of so-called retardation effects is consistent with the second order quantum electrodynamic corrections to the first order dipole-dipole C_3/R^3 potential as discussed in Refs. 75 and 76.

In principle, there are damping factors in front of each of the dispersion terms. Damping coefficients for dispersion terms have been obtained[77] from a consideration of H(1*s*)+H(1*s*) interactions[78] and verified to within ~20% by calculations on potentials for Na(3*s*)+K(4*s*) atoms,[79] for example. We are not aware of any *ab initio* calculations of damping factors explicitly for *s*+*p* atoms, but the authors of Ref. 38 have found the expressions in Ref. 77 to be useful for the $B\ ^1\Pi_u$ state of $^7Li_2$. As applied to the Na_2 *A* state, the expressions given in Ref. 77 yield damping functions that differ insignificantly from unity for $R>R_T=10.8$ Å.

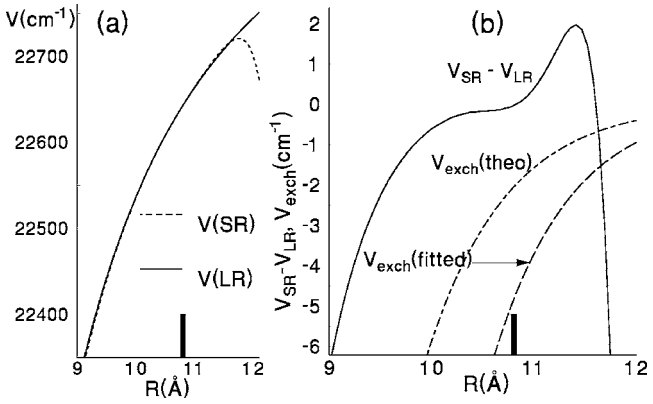

FIG. 8. (a) The fitted short-range (dashed) and long-range (solid line) potentials near the transition point R_T. (b) The difference between the short-range and long-range potentials (solid line), the theoretical exchange potential from Ref. 71 (dot-dashed line), and the fitted exchange potential (dashed line). In (a) and (b) the vertical bar denotes the *R* value of the transition point, $R_T=10.8$ Å.

The *A* state potential near the transition point R_T is shown in Fig. 8. The difference between $V_{\rm SR}(R)$ and $V_{\rm LR}(R)$ between 9.5 and 11.6 Å is less than 2 cm^{-1}, although $V(R)$ increases by about 250 cm^{-1} over this region. Because only the amplitude coefficient of the exchange potential was adjusted in the fitting process (to make the long-range potential agree with the short-range potential at R_T), the potential derivative is slightly discontinuous although the potential itself is continuous. The brief rapid rise occurs in $V_{\rm SR}$ beyond $R=R_T$ and does not appear in the actual fitted potential, which equals $V_{\rm LR}$ for $R>R_T$.

The functions C_n/R^n were fitted strictly in the region $R>R_T$. However, extensions to $R<R_T$ lead to an estimate of the exchange potential, defined to be $V_{\rm exch}=V_{\rm SR}-V_{\rm disp}$. As shown in Fig. 9(a), for these extensions, the damping corrections become significant. Both damping effects and exchange effects involve wave function overlaps, but the former are independent of electron spin, whereas the latter have the op-

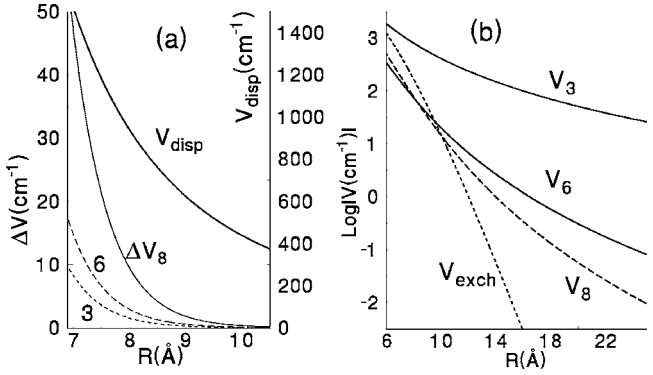

FIG. 9. (a) The sum of the contributions to $V_{\rm disp}$ as a function of *R*, together with plots of the damping corrections to V_3, V_6, and V_8, labeled 3, 6, and ΔV_8, respectively. (b) The individual components of $V_{\rm LR}$ plotted on a logarithmic scale.

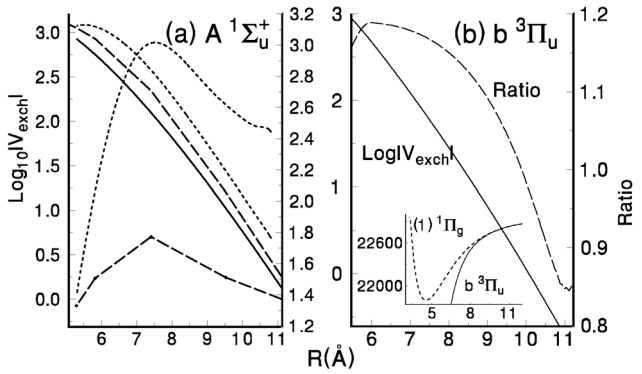

FIG. 10. (a) The monotonically decreasing functions represent the logarithm of three estimates of V_{exch} for the A state. From top to bottom, these are the experimental function, $V_{disp}-V_{SR}$ (dotted line), an *ab initio* function $(1/2)\times[V(^3\Sigma_g^+)-V(A\ ^1\Sigma_u^+]$ (from SK, dashed line), and the analytic exchange function from Ref. 71 (solid line). The peaked functions are the ratios of the first two to the last, plotted on the linear scale (right axis). (b) The logarithm of $|V_{exch}|$ for the b state obtained from one-half the difference $V(b\ ^3\Pi_u)-V[(1)\ ^1\Pi_g]$, together with the ratio of this function to the corresponding analytic exchange function from Ref. 71. The inset in (b) shows the two potentials (cm^{-1} vs Å).

posite sign for $S=0$ and 1. The individual contributions, including damping and the very small retardation effect, are shown in Fig. 9(b). Fitted values for the C_n parameters are given in Table III, including citations to *ab initio* calculations by Refs. 80–82. The uncertainties in C_6 and C_8 values from the present work are obtained from the fitting program and reflect considerable correlation effects between these two parameters, with V_{exch} and with the higher order a_i coefficients for the A state. Because the effect of the C_3 term extends to much larger values of R, this parameter is not so strongly correlated with other variables, and thus the fitting program gave an uncertainty for C_3 of only 9 parts in 4.05×10^5. An alternative estimate for the uncertainty in the reported C_3 value is provided by the difference between the value for this parameter from a fit with $R_T=10.8$ Å and another fit with $R_T=10.1$ Å that used the simpler $s+s$ form for the exchange potential. We take this difference to provide a very conservative estimate for the C_3 uncertainty since $R=10.1$ Å is further within the regime $R<R_{LR}$ so that the asymptotic expansion is even less valid here. For comparison with the C_3 value from the lifetime measurement of Ref. 83, we have used the relationship $C_3=(3\hbar/2\tau)(\lambda/2\pi)^3$. The C_3 value from the present work differs by 2σ from that in Ref. 83.

Having extracted values for V_{exch} as above, we can compare with theoretical estimates for the exchange effect. The (mostly) monotonically decreasing functions plotted on a logarithmic scale in Fig. 10(a) give, from top to bottom, values for V_{exch} from experiment as described above: one-half the difference between *ab initio* potentials for the $(1)\ ^3\Sigma_g^+$ and $A\ ^1\Sigma_u^+$ states, calculated by Kotochigova, and the exchange function calculated from the expressions in Ref. 71. The peaked functions in Fig. 10(a) give on a linear scale the ratio of the first two to the last. Clearly, the *ab initio* results agree better with the analytic exchange theory of Ref. 71 than the empirical results. We have no explanation for this. It would be interesting to compare experimental potentials for the $(1)\ ^3\Sigma_g^+$ and $A\ ^1\Sigma_u^+$ states, but, unfortunately, the available data on the former[84,85] are inadequate.

As stated above, experimental data were not available to extract information directly on the exchange potential for the $b\ ^3\Pi_u$ state. However, by the same logic as applied to the *ab initio* results presented in Fig. 10(a), we can obtain an exchange function by taking one-half the difference between the experimental potential for the $(1)\ ^1\Pi_g$ state from Ref. 86 and our extrapolated potential for the $b\ ^3\Pi_u$ state. The logarithm of the resulting function is plotted in Fig. 10(b), together with the ratio of this function to the analytic exchange function obtained from the expressions in Ref. 71. In this case, the ratio is much closer to unity.

D. Spin-orbit functions

Spin-orbit splittings and coupling terms have been observed in many molecules and have also been obtained from *ab initio* calculations for many years.[87–89] Whang *et al.*[18,19] reported spin-orbit splittings of the Na_2 $b\ ^3\Pi_u$ state for many vibrational levels and also spin-orbit coupling elements between the A and b states for many pairs of vibronic levels. In the study of the K_2 A and b states,[29] *ab initio* spin-orbit functions were scaled to fit the experimental data. Ross *et al.*[40(a)] and Sun and Huennekens[40(c)] have reported spin-orbit splittings for the NaK $b\ ^3\Pi$ state. Subsequent *ab initio* calculations[40(d),90] have qualitatively corroborated these experimental observations. Also among the alkali dimers, spin-orbit functions have been estimated empirically for RbCs (Ref. 41) and recently for NaRb [Ref. 42(b)]. In the latter case, comparisons are made with *ab initio* results. The A-b spin-orbit coupling function has also been reported for Cs_2 (Ref. 91) and scaled down for Rb_2. However, in none of these cases has there been quantitative corroboration between experimental and *ab initio* results as will be reported below.

In each of these cases involving low-lying excited states of alkali dimers, *ab initio* spin-orbit functions have exhibited a significant dip at R values somewhat greater than R_e. This has been attributed to decreasing p character of the wave function as R decreases from ∞, before the united atom regime is reached.[92] Since this R variation is clearly significant, we first attempted to fit empirical functions for both Δ_d and Δ_{od}, and these are discussed below. Eventually, *ab initio* calculations became available. However, we would like to present and discuss our empirical functions to show the merits and limitations of our approach in light of the fact that spin-orbit functions become increasingly important in heavier alkali dimers. We will then make comparisons between our empirical functions and the *ab initio* functions which are evidently quite accurate.

To extract empirical spin-orbit functions, in view of the general behavior noted above, we assumed functions of the form of a Morse curve for both Δ_d and Δ_{od}:

$$\Delta_i(R)=p_i(1)+[p_i(2)-p_i(1)][1-e^{p_i(3)[p_i(4)-R]}]^2. \quad (7)$$

The asymptotic values [$p_i(2)$ in this expression] are known to be $\Delta/3$ for Δ_d and $\sqrt{2}\Delta/3$ for Δ_{od}, where Δ is the atomic fine structure interval, which is 17.196(1) cm^{-1} (Ref. 65) for the Na $3\ ^2P$ state. This leaves three unknown parameters.

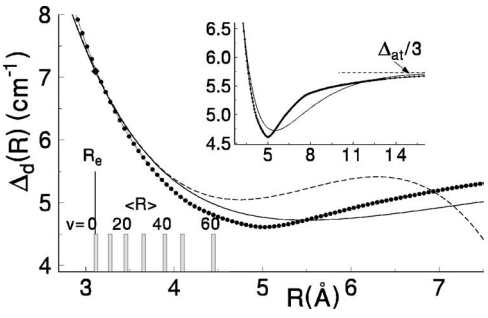

FIG. 11. Diagonal b state spin-orbit function Δ_d. The dashed line denotes results of a fit to a Taylor series expansion about R_e that is made possible by the range of values of $\langle v|R|v\rangle$ as a function of vibrational level as indicated below the curve. The solid line denotes the best fit to a Morse function [Eq. (7)] adjusted to match the Taylor series expansion as closely as possible. The filled circles and connecting line denote *ab initio* results. The inset shows an overview of the asymptotic region.

For Δ_d, the different vibrational levels of the b state provided a range of values of $\langle R\rangle$, so that R dependence could be extracted. Because it is cumbersome to adjust the Morse function, Eq. (7) itself, it was simpler to introduce a Taylor series expansion about $R=R_e$, and fit as many coefficients as possible. Then, parameters for the Morse function were determined by matching the behavior near R_e. Figure 11 shows the values of $\langle v|R|v\rangle$ for various v, the Taylor series function, and the resultant Morse function for Δ_d. The *ab initio* spin-orbit function, shown with filled circles and connecting lines in Fig. 11, lies quite close to the empirical results near R_e, and is undoubtedly more reliable at other values.

For Δ_{od}, as discussed in Refs. 67 and 93, matrix elements between near degenerate levels reflect the phase accumulation at the stationary phase point, which is effectively at the potential crossing point R_x. Accordingly, our empirical values for the off-diagonal spin-orbit function reflected its value only at R_x, and each of the solid-line curves in Fig. 12 pass through very nearly the same value at R_x and give comparably good fit results. The values at R_x happen to agree well with the value of the *ab initio* function at that point. In the final data fits reported here, the *ab initio* function for Δ_{od} is used. Numerical values are given in the EPAPS file.[43]

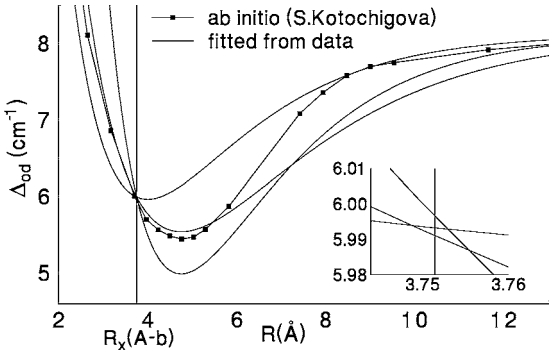

FIG. 12. Off-diagonal A-b spin-orbit coupling functions. The solid-line curves show various fitted Morse function expressions. Each of these curves gives a comparably good fit to the experimental data. The inset shows that they cross within a small region near the crossing point of the A and b state potentials. The connected squares denote the *ab initio* results of SK which were used in the final fit.

We now summarize the methods used to calculate the spin-orbit functions. Since spin-orbit interaction is a relativistic effect, in principle, it must be calculated by using Dirac's relativistic formalism. The reduction of Dirac's relativistic equation to nonrelativistic form leads to the spin-orbit energy for a one-electron atom, which can then be generalized to many-electron atoms and molecules. This approximation is often used to calculate the spin-orbit coupling matrix elements based on nonrelativistic wave functions. In the current study we carried out such a nonrelativistic treatment of the spin-orbit interaction. *Ab initio* nonrelativistic valence bond theory is applied to calculate the electronic wave functions of alkali dimer Na_2. The valence bond method is very suitable for studying molecules over a wide range of internuclear separations. It naturally provides a physically realistic description of atoms at large R. At the same time, the modern development of the method permits an accurate description of a molecule at short and intermediate separations R.[94]

The basis functions in our version of the method are obtained numerically by solving a set of integrodifferential Hartree-Fock equations for each atom. The molecular wave function, which includes electron correlations, is most commonly constructed from basis functions that contain excitations of one, two, or three electrons into virtual states. However, describing these excited virtual states using the Hartree-Fock wave functions is known to result in rather slow and often nonuniform convergence. Moreover, a complete set of these functions has to contain continuum functions which are computationally impractical. Our solution of this problem is to use a set of Sturmian functions to model virtual state correlation in a molecule. These discrete functions form a complete set and have an asymptotic behavior and orbital size that is similar to the occupied valence orbitals. The excitations into virtual states involve both excitations from valence and core shells. The latter is known to be responsible for the core-valence or core-polarization interactions.

In our approach, the correlated molecular wave function is obtained by a direct configuration interaction (CI) method with explicit construction of configurations with single, double, and triple excitations from the reference configuration. In general, to make a reliable prediction for molecular properties the number of configurations has to be very large. In many cases, the number of configurations can be reduced by a perturbative estimate of the contribution of excited configurations on the needed molecular wave function. If the contribution is below a threshold value, the corresponding excited configuration is omitted from the CI calculation.

For the *ab initio* calculation of spin-orbit coupling effects, we use the nonrelativistic spin-orbit Hamiltonian.[88,89] The Hamiltonian in atomic units is given by

$$\hat{H}_{SO}=\frac{\alpha^2}{2}\sum_N\sum_i\frac{Z_N}{r_{iN}^3}(\mathbf{r}_{iN}\times\mathbf{p}_i)\mathbf{s}_i-\frac{\alpha^2}{2}\times\sum_{i\neq j}\frac{1}{r_{ij}^3}[\mathbf{r}_{ij}\times\mathbf{p}_i](\mathbf{s}_i+2\mathbf{s}_j). \quad (8)$$

The first term in Eq. (8) is a one-electron operator, which describes the "spin-same-orbit" interaction, whereas the sec-

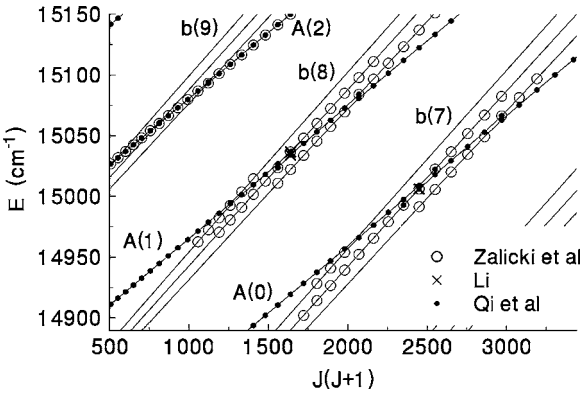

FIG. 13. Calculated and observed term values showing the extent of the data in the region of *A*-*b* perturbations for low v levels of the *A* state.

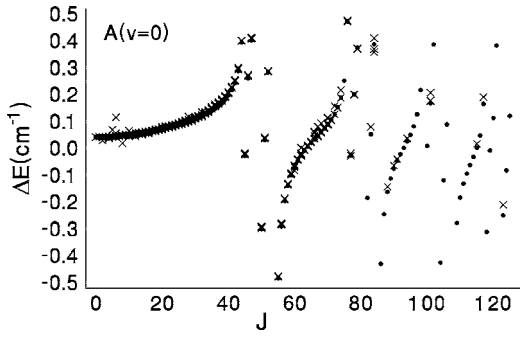

FIG. 14. Calculated (circles) and observed (crosses) term values for $v=0$ of the *A* state with the deperturbed $E(v=0,J)$ values subtracted. The quality of the fit is shown on an expanded scale relative to the previous figure. Divergences appear at the perturbation crossings.

ond (two-electron) term in Eq. (8) features the "spin-other-orbit" interaction. Z_N is the charge on nucleus N, r_{iN} denotes the distance between the Nth nucleus and the ith electron, r_{ij} denotes interelectron distance, and **s** and **p** define spin and momentum operators. The constant α is the fine structure constant.

To evaluate the one-electron and two-electron matrix elements of Eq. (8), we have only to consider molecular states that differ from each other by zero, one, or two spin-orbitals. The matrix elements of the one-electron operator are taken over all occupied atomic orbitals and make the larger contribution to the spin-orbit coupling energy than do the two-electron matrix elements.

In the alkali-metal dimer Na_2, the spin-orbit operator H_{SO} couples the nonrelativistic $A\,^1\Sigma_u^+$ and $b\,^3\Pi_u$ potentials and creates a mixing mechanism for the vibrational levels of $A\,^1\Sigma_u^+$ and $b\,^3\Pi_u$ states. We have calculated the diagonal $\Delta_d=\langle b\,^3\Pi_u|H_{SO}|b\,^3\Pi_u\rangle$ and off-diagonal $\Delta_{od}=\langle b\,^3\Pi_u|H_{SO}|A\,^1\Sigma_u^+\rangle$ matrix elements. At large internuclear separations the matrix elements approach the constant values of $\Delta_{atomic}/3=5.7321\ cm^{-1}$ for Δ_d and $\sqrt{2}\Delta_{atomic}/3=8.1064\ cm^{-1}$ for Δ_{od}. Our theoretical values beyond 13 Å lie slightly below the asymptotic value, but the calculated function extrapolates to the expected values with no external adjustment as was required for the K_2 spin-orbit functions in Ref. 29.

To optimize the fit of calculated eigenvalues to the experimental term values, these spin-orbit functions were multiplied by a scaling function, $f_{SO}=1+q_2\exp(-q_3R)$, and the q_i parameters were adjusted in the least squares fit. For $\Delta_d(\Delta_{od})$, q_3 was taken to be 0.17 (0.20) $Å^{-1}$, while the optimum values for q_2 were found to be −0.0085(1) and 0.0186(7), respectively. Thus, the correction factor for Δ_d at $R=R_e$ was 0.9950(1), and for Δ_{od} at $R=R_x$ it was 1.0087(3). Since each of these factors is close to unity, they indicate that the *ab initio* function itself was highly consistent with the data. The correction factors are indistinguishable from unity on the scale of Figs. 11 and 12. We attribute the good agreement with the molecular spectroscopy data and with the known large R limits for Na $3\,^2P$ atoms to the inclusion of core excitations and also to the fact that there are fewer electrons in Na_2 than in heavier alkali atoms.

E. Calculated term values

Plots of calculated and observed term values make it possible to assess the extent of the data in various perturbation regions, as illustrated in Fig. 13. The vertical scale of this figure is of course too large to reveal the quality of the fit to the data. An alternative perspective is given in the next figure, Fig. 14, in which the deperturbed energies are subtracted from observed and calculated eigenvalues for the $v=0$ level of the *A* state. For a more detailed evaluation of the quality of the fit in such a region, listings of observed and fitted term values are available in the EPAPS files.

Similar plots over a wider region of energy and rotation demonstrate the value of the DVR matrix approach. Figure 15 shows that over the range of the observed rotational levels, there are many crossings between *A* and *b* state vibronic levels. In Refs. 15 and 16, two perturbation crossings were modeled. Clearly when there are perturbation crossings, and the data extend to larger values of J, the band-by-band analysis becomes problematic.

In Table IV, we list previous estimates (columns 2–4) as well as our own deperturbed $G(v)$ values (column 5) for the *A* state together with the $J=0$ perturbation shifts, $B(v)$ values, and turning points. These deperturbed values are simply the DVR eigenvalues for $J=0$ calculated from the deperturbed *A* state potential at the energies given in column 5, with no coupling to the *b* state. The shifts are the $J=0$ term

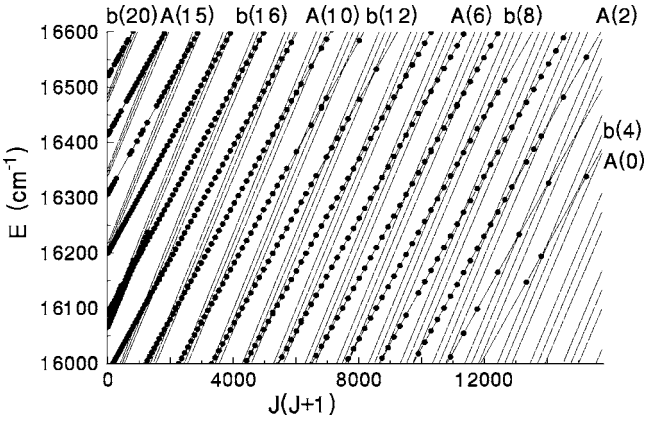

FIG. 15. Calculated and observed term values over a larger region. In this figure, the filled dots represent experimental data from any of the sources.

TABLE IV. Deperturbed $G(v)$ values, from previous studies and this one, perturbation shifts, $B(v)$ values, and turning points for the A state. PS=DVR eigenvalue for $J=0$ minus the deperturbed value, $G(v)=\tilde{G}(v)+2B(v)$. The last two columns give the inner and outer turning points at the energies given in column 5. All quantities are in cm^{-1} except for $R_{\pm}$ which are in Å.

v	Previous work $G(v)$			$\tilde{G}(v)+2B(v)$	PS	$B(v)$	R_-	R_+
0	14 739.110[a]	14 739.1210(40)[b]	14 739.040(17)[c]	14 739.0057	0.0420	0.110 553 9	3.485 415 8	3.802 640 2
1	14 855.717[a]	14 855.7039(22)[b]	14 855.653(18)[c]	14 855.6595	0.0016	0.109 993 2	3.382 091 4	3.932 170 2
2	14 971.612[a]	14 971.6633(40)[b]	14 971.595(8)[c]	14 971.5844	−0.0174	0.109 435 1	3.314 355 3	4.026 166 1
3	15 086.798[a]	15 086.8260(12)[b]	15 086.786(10)[c]	15 086.7836	0.1187	0.108 879 2	3.261 205 9	4.105 604 4
4	15 201.272[a]	15 201.2777(28)[b]		15 201.2605	−0.0952	0.108 325 6	3.216 761 3	4.176 581 5
5	15 315.037[a]	15 315.0847(6)[b]		15 315.0179	−0.0416	0.107 774 0	3.177 989 6	4.241 883 7
6	15 428.090[a]	15 428.1629(20)[b]		15 428.0586	0.0025	0.107 224 3	3.143 455 5	4.303 061 4
7	15 540.432[a]	15 540.4948(50)[b]		15 540.3852	0.0552	0.106 676 5	3.112 187 3	4.361 082 4
8	15 652.064[a]			15 652.0002	0.5425	0.106 130 3	3.083 430 5	4.416 598 7
9	15 762.984[a]	15 762.9985(72)[b]		15 762.9059	−0.0205	0.105 585 6	3.057 087 1	4.470 074 6
10	15 873.193[a]	15 873.2250(29)[b]		15 873.1044	0.0100	0.105 042 3	3.032 412 2	4.521 854 5
11				15 982.5976	0.0131	0.104 500 4	3.009 296 8	4.572 202 7
12				16 091.3872	0.0075	0.103 959 5	2.987 531 6	4.621 326 9
13				16 199.4750	−0.0028	0.103 419 8	2.966 951 7	4.669 394 7
14	16 306.926[d]			16 306.8623	−0.0094	0.102 880 9	2.947 421 7	4.716 543 2
15	16 413.614[d]			16 413.5505	−0.0140	0.102 342 9	2.928 831 3	4.762 886 4
16	16 519.603[d]			16 519.5408	−0.0121	0.101 805 5	2.911 087 0	4.808 521 1
17	16 624.894[d]			16 624.8340	0.0115	0.101 268 7	2.894 107 8	4.853 529 5
18	16 729.489[d]			16 729.4311	−0.0758	0.100 732 3	2.877 847 0	4.897 983 2
19	16 833.389[d]			16 833.3327	−0.0293	0.100 196 3	2.862 208 1	4.941 944 2
20	16 936.596[d]			16 936.5394	−0.0108	0.099 660 5	2.847 165 8	4.985 467 6
21	17 039.110[d]			17 039.0514	0.0124	0.099 124 7	2.832 670 6	5.028 601 8
22	17 140.932[d]			17 140.8691	0.1260	0.098 588 9	2.818 671 7	5.071 390 7
23	17 242.062[d]			17 241.9924	−0.0423	0.098 053 0	2.805 184 1	5.113 873 6
24	17 342.502[d]			17 342.4213	−0.0069	0.097 516 8	2.792 111 7	5.156 086 4
25	17 442.251[d]			17 442.1554	0.0091	0.096 980 2	2.779 456 4	5.198 061 8
26	17 541.310[d]			17 541.1944	0.0274	0.096 443 0	2.767 190 6	5.239 829 9
27	17 639.678[d]			17 639.5375	−0.1271	0.095 905 2	2.755 312 3	5.281 418 7
28	17 737.356[d]			17 737.1840	−0.0043	0.095 366 6	2.743 747 1	5.322 854 4
29	17 834.343[d]			17 834.1328	0.0036	0.094 827 0	2.732 523 4	5.364 161 3
30	17 930.637[d]			17 930.3829	0.0057	0.094 286 4	2.721 611 0	5.405 362 7
31	18 026.238[d]		18 025.95(4)[e]	18 025.9328	0.0089	0.093 744 5	2.710 993 4	5.446 480 5
32	18 121.144[d]		18 120.81(1)[e]	18 120.7809	−0.0037	0.093 201 3	2.700 658 3	5.487 535 4
33	18 215.354[d]			18 214.9255	−0.0033	0.092 656 5	2.690 589 3	5.528 548 0
34	18 308.865[d]		18 308.37(1)[e]	18 308.3646	−0.0053	0.092 110 1	2.680 775 8	5.569 537 3
35	18 401.675[d]		18 401.10(1)[e]	18 401.0959	−0.0072	0.091 561 7	2.671 206 5	5.610 522 7
36	18 493.781[d]		18 493.10(2)[e]	18 493.1170	−0.0377	0.091 011 3	2.661 873 9	5.651 522 2
37	18 585.179[d]		18 584.44(1)[e]	18 584.4252	−0.0127	0.090 458 4	2.652 753 8	5.692 548 8
38	18 675.866[d]			18 675.0176	−0.0128	0.089 903 7	2.643 863 3	5.733 636 7
39	18 765.838[d]		18 764.92(1)[e]	18 764.8908	−0.0110	0.089 346 1	2.635 173 5	5.774 787 2
40	18 855.091[d]		18 854.12(3)[e]	18 854.0415	0.0010	0.088 785 6	2.626 681 9	5.816 023 5
41	18 943.619[d]		18 942.48(1)[e]	18 942.4659	−0.0312	0.088 222 1	2.618 386 3	5.857 363 5
42	19 031.416[d]		19 030.20(1)[e]	19 030.1600	−0.0190	0.087 655 3	2.610 271 5	5.898 824 8
43	19 118.477[d]			19 117.1193	−0.0127	0.087 085 0	2.602 336 2	5.940 425 6
44			19 203.29(1)[e]	19 203.3393	−0.0015	0.086 510 9	2.594 573 3	5.982 184 2
45			19 288.72(5)[e]	19 288.8149	−0.2834	0.085 932 9	2.587 003 7	6.024 119 1
46			19 373.52(1)[e]	19 373.5408	−0.0262	0.085 350 6	2.579 548 6	6.066 249 6
47				19 457.5114	−0.0142	0.084 763 7	2.572 272 4	6.108 595 0
48			19 540.66(4)[e]	19 540.7206	−0.0036	0.084 171 9	2.565 149 1	6.151 175 6
49			19 623.23(7)[e]	19 623.1620	0.0311	0.083 575 0	2.558 172 3	6.194 011 9
50			19 704.81(4)[e]	19 704.8287	−0.0408	0.082 972 6	2.551 348 8	6.237 125 7

[a]Calculated from the Y_{ij} parameters of Ref. 8.
[b]Reference 15.
[c]Reference 20.
[d]Reference 9.
[e]Reference 18.

values from the full multichannel DVR matrix calculation less these single channel, deperturbed eigenvalues, and $B(v)=\langle\psi(v)|\hbar^2/2\mu R^2|\psi(v)\rangle/(100hc)$ (in cm^{-1}), where $\psi(v)$ is the DVR single channel eigenfunction for $J=0$ and μ is the reduced mass. As shown in Fig. 14, the perturbation shifts vary considerably with J, so the sixth column in Table IV gives only a rough indication of perturbation effects. Note that as the data used to analyze the perturbations become more extensive, in the progression from columns 2 to 5, the estimate of the deperturbed vibrational energies gradually decreases, at least for the lower v levels. For these levels, the effect of coupling with remote levels of the b state is to raise the observed energies of the A state levels. The deperturbation procedure therefore leads to lower energies. Note also that the uncoupled A state potential in this table near $v=15$ differs by more than 10 cm^{-1} from the RKR potential of Ref. 23, which was based on much less complete data for low v, but which is accurate for $v>50$. However, any single channel representation ultimately fails for the Na_2 A state as discussed earlier. The turning points present in Table IV represent the lower part of a Born-Oppenheimer potential, which must be combined with spin-orbit coupling functions to model the spectroscopic data accurately. Near the dissociation limit, the spin-orbit functions are larger than the nonrelativistic binding energy. Photoassociation data for Rb_2 showed mixing between the two series of 0_u^+ levels tending to the $5P_{1/2}$ and $5P_{3/2}$ limits,[95] manifested in higher $B(v)$ values for those states with large $P_{3/2}$ components. A study of the Na_2 data from Ref. 23 revealed only one possible such case, with just a slight elevation of $B(v)$ relative to the adjacent levels near where a $P_{3/2}$ state was predicted to be.

For the b state, $G(v)$ values and RKR turning points for $v\leqslant 57$ in Ref. 18 agree with present results, after slight differences of the model are taken into account.

Although not discussed here, hyperfine structure in the $b\,^3\Pi_u$ and in mixed A b states has been observed in Refs. 20, 23, 96, and 97 and in detailed observations of photoassociation of laser-cooled Na atoms.[98] An interesting general statement about b state hyperfine effects was presented in Ref. 99 and explained about the same time in Ref. 100; the hyperfine coupling parameter obtained from observations of b state levels (and from many other Na_2 triplet state levels) is very nearly one-fourth the Na atomic Fermi contact interaction of 885.8 MHz (Ref. 101) (one-half the atomic $3S$ state hyperfine splitting).

IV. CONCLUSION

We have compiled most of the older laser spectroscopy data on the $A\,^1\Sigma_u^+$ and $b\,^3\Pi_u$ states of Na_2 together with several sets of unpublished data, including new sub-Doppler measurements of some 15 000 $A\leftarrow X$ transitions. Although the data on the b state extend no higher than $v=57$, the A state data go essentially to the dissociation limit. The present analysis, however, neglects hyperfine structure and thus has been applied only up to 0.15 cm^{-1} below the $3\,^2S+3\,^2P_{1/2}$ hyperfine center of gravity. This range of data, together with *ab initio* spin-orbit functions, allows us to fit both short-range and long-range (dispersion and exchange) potential parameters for the A state.

This compilation of available data reveals areas where the data are not plentiful or lacking. For example, no levels of the $b\,^3\Pi_u$ state have been identified above $v=57$ (at 20 700 cm^{-1}). Also since data on only two or three rotational states per vibrational level of the A state are available between $v=51$ and 100, there may be perturbation shifts that are not accurately characterized in this region.

Regarding the exchange potential, it is pertinent to note that although there have been careful tests that have validated exchange theory for the potential differences between $X\,^1\Sigma_g^+$ and $a\,^3\Sigma_u^+$ molecular states arising from ^2S ground state alkali atoms, as in Ref. 102, for molecular states arising from $^2S+^2P$ atoms, there exist detailed theoretical discussions of exchange effects,[71,73] but experimental data have been inadequate for a definitive test to our knowledge. For the A state of Na_2, experimental data presented here are unusually complete. We have extracted values for V_{exch} for both the A and b states by various methods to focus attention on these functions. The exchange potential for the b state from $V_{\text{exch}}=(1/2)[V(b\,^3\Pi_u)-V((1)\,^1\Pi_g)]$, estimated over the range $6\leqslant R\leqslant 11$ Å, lies within 20% of the analytic results from Ref. 71. [For this purpose, the b state potential was extrapolated beyond the range of available data, while the $(1)\,^1\Pi_g$ potential is well determined experimentally.] However, an estimate for the A state, $V_{\text{exch}}=V_{\text{disp}}-V_{\text{SR}}$ over the same range of R is 2.4–3.0 times the analytic results of Ref. 71. More extensive experimental data on the $(1)\,^3\Sigma_g^+$ state might lead to a better empirical estimate from the relation $V_{\text{exch}}(A)=(1/2)[V((1)\,^3\Sigma_g^+)-V(A\,^1\Sigma_u^+)]$.

This study is intended in part as a test demonstration of DVR matrix methods for modeling diatomic spectra, following earlier work on K_2.[27,29] The results of the analysis are summarized by the Hund's case a Born-Oppenheimer potentials plus spin-orbit coupling functions. Sufficiently far from the asymptotic regime, the potentials are close to what one would obtain from a RKR approach based on deperturbed $G(v)$ and $B(v)$ values. Diagonalization of the DVR matrix for each value of J yields eigenvalues and composition of each level. Centrifugal distortion effects are included in these term values without requiring explicit additional parameters. The change in coupling from Hund's case a to case c near the dissociation limit is also implicit in the DVR Hamiltonian matrix. Further study is needed to determine whether the residual deviations between observation and the DVR eigenvalues reflects failures of the DVR model or artifacts of line measurement processes and/or calibrations, which are especially critical for multistep laser spectroscopy. Extensive tables of potentials and data, and plots of observed and calculated term values up to $v=32$ of the A state, are available in the EPAPS file.[43]

The perturbative interactions between the A and b states of Na_2 are not large effects. We hope that the modeling and analysis techniques presented here will help in the development of techniques to address the stronger perturbative interactions in heavier alkali dimers.

ACKNOWLEDGMENTS

The authors are very grateful to M. Aubert-Frécon for communications regarding the exchange potential, to W. Zemke for discussions on matching the short-range and long-range potentials, and to B. Beser (a graduate student at Temple University) for detecting a flaw in our *A* state potential at one point. The authors are pleased to acknowledge support by NSF (Temple University, Stony Brook, and MIT), AOR (Temple and SB) and ONR (SB).

[1] See, for example *Ultracold Polar Molecules: Formation and Collisions*, special issue of Eur. Phys. J. D **31**, No. 2 (2004); *Special Issue on Cold Molecules*, J. Phys. B **39**, No. 39 (2006).
[2] L. Li and A. M. Lyyra, Spectrochim. Acta, Part A **55**, 2147 (1999) on the use of window states to excite higher triplet states of Li_2 and Na_2.
[3] R. W. Wood and F. E. Hackett, Astrophys. J. **30**, 339 (1909).
[4] W. R. Fredrickson and C. R. Stannard, Phys. Rev. **44**, 632 (1933).
[5] R. S. Mulliken, Rev. Mod. Phys. **4**, 1 (1932).
[6] T. Carroll, Phys. Rev. **52**, 822 (1937).
[7] L. Li, S. F. Rice, and R. W. Field, J. Mol. Spectrosc. **105**, 344 (1984).
[8] P. Kusch and M. M. Hessel, J. Chem. Phys. **63**, 4087 (1975).
[9] M. Kaminsky, thesis, Stanford University, 1976.
[10] M. E. Kaminsky, R. T. Hawkins, F. V. Kowalski, and A. L. Schawlow, Phys. Rev. Lett. **36**, 671 (1976).
[11] F. Engelke, H. Hage, and C. D. Caldwell, Chem. Phys. **64**, 221 (1982).
[12] J. B. Atkinson, Ph.D. thesis, Universität Kaiserslautern, 1982.
[13] J. B. Atkinson, J. Becker, and W. Demtröder, Chem. Phys. Lett. **87**, 92 (1982).
[14] K. Shimizu and F. Shimizu, J. Chem. Phys. **76**, 1126 (1983).
[15] C. Effantin, O. Babaky, K. Hussein, J. d'Incan, and R. F. Barrow, J. Phys. B **18**, 4077 (1985).
[16] O. Babaky, thèse, Université Claude Bernard, Lyon, 1986.
[17] A. M. Lyyra, H. Wang, T.-J. Whang, and W. C. Stwalley, Phys. Rev. Lett. **66**, 2724 (1991).
[18] T.-J. Whang, W. C. Stwalley, L. Li, and A. M. Lyyra, J. Chem. Phys. **97**, 7211 (1992).
[19] T.-J. Whang, thesis, University of Iowa, 1991.
[20] P. Zalicki, J. Vigué, C. Effantin, and A. Bernard, unpublished manuscript (1993).
[21] G. Chawla, thesis, MIT, 1985.
[22] M. S. Schweda, G. K. Chawla, and R. W. Field, Opt. Commun. **42**, 165 (1982); S. Churassy, G. K. Chawla, and R. W. Field, J. Opt. Soc. Am. B **2**, 1929 (1985).
[23] E. Tiemann, H. Knöckel, and H. Richling, Z. Phys. D: At., Mol. Clusters **37**, 323 (1996).
[24] P. Qi, thesis, Temple University, 2007.
[25] J. Y. Seto, R. J. Le Roy, J. Vergès, and C. Amiot, J. Chem. Phys. **113**, 3067 (2000).
[26] J. A. Coxon and T. C. Melville, J. Mol. Spectrosc. **235**, 235 (2006).
[27] Ch. Lisdat, O. Dulieu, H. Knöckel, and E. Tiemann, Eur. Phys. J. D **17**, 319 (2001).
[28] O. Docenko, M. Tamanis, R. Ferber, A. Pashov, H. Knöckel, and E. Tiemann, Eur. Phys. J. D **31**, 205 (2004).
[29] M. R. Manaa, A. J. Ross, F. Martin, P. Crozet, A. M. Lyyra, L. Li, C. Amiot, and T. Bergeman, J. Chem. Phys. **117**, 11208 (2002).
[30] R. Meyer, J. Chem. Phys. **52**, 2053 (1970).
[31] D. Colbert and W. H. Miller, J. Chem. Phys. **96**, 1982 (1992).
[32] O. Dulieu and P. S. Julienne, J. Chem. Phys. **103**, 60 (1995).
[33] R. Kosloff, J. Phys. Chem. **92**, 2087 (1988).
[34] V. Kokoouline, O. Dulieu, R. Kosloff, and F. Masnou-Seeuws, J. Chem. Phys. **110**, 9865 (1999).
[35] E. Tiesinga, C. J. Williams, and P. S. Julienne, Phys. Rev. A **57**, 4257 (1998).
[36] P. Kusch and M. M. Hessel, J. Chem. Phys. **67**, 586 (1977); C. Linton, R. Bacis, P. Crozet, F. Martin, A. J. Ross, and J. Vergès, J. Mol. Spectrosc. **151**, 159 (1992); K. Urbanski, S. Antonova, A. Yiannopoulou, A. M. Lyyra, L. Li, and W. C. Stwalley, J. Chem. Phys. **104**, 2813 (1886); C. Linton, F. Martin, I. Russier, A. J. Ross, P. Crozet, S. Churassy, and R. Bacis, J. Mol. Spectrosc. **175**, 340 (1996); X. Wang, J. Yang, J. Qi, and A. M. Lyyra, *ibid.* **191**, 295 (1998); X. Wang, J. Magnes, A. M. Lyyra, A. J. Ross, F. Martin, P. M. Dove, and R. J. Le Roy, J. Chem. Phys. **117**, 9339 (2002); A. Adohi-Krou, F. Martin, A. J. Ross, C. Linton, and R. J. Le Roy, *ibid.* **121**, 6309 (2004).
[37] F. Martin, M. Aubert-Frécon, R. Bacis, P. Crozet, C. Linton, S. Magnier, A. J. Ross, and I. Russier, Phys. Rev. A **55**, 3458 (1997).
[38] N. Bouloufa, P. Cacciani, R. Vetter, A. Yiannopoulou, F. Martin, and A. J. Ross, J. Chem. Phys. **114**, 8445 (2001).
[39] St. Falke, I. Sherstov, E. Tiemann, and Ch. Lisdat, J. Chem. Phys. **125**, 224303 (2006).
[40] (a) A. J. Ross, C. Effantin, J. d'Incan, and R. F. Barrow, J. Phys. B **19**, 1449 (1986); (b) P. Kowalczyk, J. Chem. Phys. **91**, 2779 (1989); (c) H. Sun and J. Huennekens, *ibid.* **97**, 4714 (1992); (d) R. Ferber, E. A. Pazyuk, A. V. Stolyarov, A. Zaitsevskii, P. Kowalczyk, H. Chen, H. Wang, and W. C. Stwalley, *ibid.* **112**, 5740 (2000); (e) P. Burns, A. D. Wilkins, A. P. Hickman, and J. Huennekens, *ibid.* **122**, 074306 (2005).
[41] T. Bergeman, C. E. Fellows, R. F. Gutterres, and C. Amiot, Phys. Rev. A **67**, 050501 (2003).
[42] M. Tamanis, R. Ferber, A. Zaitsevskii, E. A. Pazyuk, A. V. Stolyarov, H. Chen, J. Qi, H. Wang, and W. C. Stwalley, J. Chem. Phys. **117**, 7980 (2002); O. Docenko, M. Tamanis, R. Ferber, E. A. Pazyuk, A. Zaitsevskii, A. V. Stolyarov, A. Pashov, H. Knöckel, and E. Tiemann, Phys. Rev. A **75**, 042503 (2007). See also publisher's note Phys. Rev. A **75**, 059907(E) (2007).
[43] See EPAPS Document No. E-JCPSA6-127-001725 for data files associated with this paper. This document can be reached via a direct link in the online article's HTML reference section or via the EPAPS homepage (http://www.aip.org/pubservs/epaps.html).
[44] R. N. Ahmad-Bitar and A. S. Al-Ayash, J. Mol. Spectrosc. **106**, 299 (1984).
[45] G. Gerber and R. Möller, Chem. Phys. Lett. **113**, 546 (1985).
[46] M. Li, C. Wang, Y. Wang, and L. Li, J. Mol. Spectrosc. **123**, 161 (1987).
[47] H. Katô, M. Otani, and M. Baba, J. Chem. Phys. **89**, 653 (1988).
[48] H. Wang, thesis, University of Iowa, 1991.
[49] B. Ji, thesis, University of Iowa, 1995.
[50] H.-G. Krämer, M. Keil, R. A. Bernheim, and W. Demtröder, Chem. Phys. Lett. **272**, 391 (1997).
[51] P. Zalicki, N. Billy, G. Gouédard, and J. Vigué, J. Chem. Phys. **99**, 6436 (1993).
[52] M. Raab, G. Höning, and W. Demtröder, J. Chem. Phys. **76**, 4370 (1982).
[53] A. M. Lyyra, W. T. Luh, L. Li, H. Wang, and W. C. Stwalley, J. Chem. Phys. **92**, 43 (1990).
[54] A. Grochola, W. Jastrzebski, and P. Kowalczyk, J. Mol. Spectrosc. **232**, 291 (2005).
[55] A. Grochola, W. Jastrzebski, and P. Kowalczyk, Mol. Phys. **104**, 2569 (2006).
[56] C. Wieman and T. W. Hänsch, Phys. Rev. Lett. **36**, 1170 (1976).
[57] V. Stert and R. Fischer, Appl. Phys. **17**, 151 (1978).
[58] W. Demtröder, *Laser Spectroscopy: Basic Concepts and Instrumentation* (Springer, Berlin, 2003).
[59] The Aimé Cotton Iodine Atlas, S. Gerstenkorn and P. Luc, *Atlas du Spectre d'Absorption de la Molecule d'Iode*, Editions du CNRS, Paris, 1978, was recalibrated in 1979 (next reference).
[60] S. Gerstenkorn and P. Luc, Rev. Phys. Appl. **14**, 791 (1979).
[61] H. Knöckel, B. Bodermann, and E. Tiemann, Eur. Phys. J. D **28**, 199 (2004).
[62] P. Kusch and M. M. Hessel, J. Chem. Phys. **68**, 2591 (1978).
[63] O. Babaky and K. Hussein, Can. J. Phys. **67**, 9112 (1989).
[64] K. M. Jones, S. Maleki, S. Bize *et al.*, Phys. Rev. A **54**, R1006 (1996).
[65] P. Juncar, J. Pinard, J. Hamon, and A. Chartier, Metrologia **17**, 77 (1981).
[66] E. Ahmed, A. Hansson, P. Qi, T. Kirova, A. Lazoudis, S. Kotochigova, A. M. Lyyra, L. Li, J. Qi, and S. Magnier, J. Chem. Phys. **124**, 084308 (2006).
[67] R. W. Field and H. Lefebvre-Brion, *The Spectra and Dynamics of Diatomic Molecules* (Elsevier, Amsterdam, 2004).
[68] T. Bergeman, P. S. Julienne, C. J. Williams, E. Tiesinga, M. R. Manaa, H. Wang, P. L. Gould, and W. C. Stwalley, J. Chem. Phys. **117**, 7491 (2002).
[69] R. J. Le Roy, Can. J. Phys. **52**, 246 (1974).
[70] B. Ji, C.-C. Tsai, and W. C. Stwalley, Chem. Phys. Lett. **236**, 242 (1995).
[71] O. Bouty, G. Hadinger, and M. Aubert-Frécon, J. Mol. Struct.: THEOCHEM **330**, 97 (1995).
[72] S. J. Umanskii and A. I. Voronin, Theor. Chim. Acta **12**, 166 (1968).
[73] G. Hadinger, G. Hadinger, O. Bouty, and M. Aubert-Frécon, Phys. Rev.

A **50**, 1927 (1994); M. Aubert-Frécon, S. Magnier, and S. Rousseau, J. Mol. Spectrosc. **188**, 182 (1998).
[74] M. Aubert-Frécon (private communication).
[75] J. O. Hirschfelder and W. J. Meath, in *Advances in Chemical Physics*, edited by J. O. Hirschfelder (Interscience, New York, 1967), Vol. XII.
[76] E. A. Power, in *Advances in Chemical Physics*, edited by J. O. Hirschfelder (Interscience, New York, 1967), Vol. XII.
[77] A. J. C. Varandas and A. I. Voronin, Mol. Phys. **85**, 497 (1995).
[78] A. Koide, W. J. Meath, and A. R. Allnatt, Chem. Phys. **58**, 105 (1981).
[79] K. Hussein and M. Aubert-Frécon, Can. J. Phys. **73**, 537 (1995).
[80] B. Bussery and M. Aubert-Frécon, J. Chem. Phys. **82**, 3224 (1985).
[81] F. Vigne-Maeder, Chem. Phys. **85**, 139 (1984).
[82] M. Marinescu and A. Dalgarno, Z. Phys. D: At., Mol. Clusters **36**, 239 (1996).
[83] U. Volz, M. Marjerus, H. Liebel, A. Schmitt, and H. Schmoranzer, Phys. Rev. Lett. **76**, 2862 (1996).
[84] A. Färbert, J. Koch, T. Platz, and W. Demtröder, Chem. Phys. Lett. **223**, 546 (1994); A. Färbert, P. Kowalczyk, H. v. Busch, and W. Demtröder, *ibid.* **252**, 243 (1996).
[85] K. Xu, Y. Liu, J. R. Abo-Shaeer, T. Mukaiyama, J. K. Chin, D. E. Miller, W. Ketterle, K. M. Jones, and E. Tiesinga, Phys. Rev. A **72**, 043604 (2005).
[86] C. Effantin, J. d'Incan, A. R. Ross, R. F. Barrow, and J. Vergès, J. Phys. B **17**, 1515 (1984).
[87] S. R. Langhoff, M. L. Sink, R. H. Pritchard, and C. W. Kern, J. Mol. Spectrosc. **96**, 200 (1982).
[88] W. G. Richards, H. P. Trivedi, and D. L. Cooper, *Spin-orbit Coupling in Molecules* (Clarendon, Oxford, 1981), p. 105.
[89] B. A. Hess, C. M. Marian, and S. D. Peyerimhoff, in *Modern Electronic Structure Theory*, edited by D. R. Yarkony (World Scientific, Singapore, 1995), Pt. 1, pp. 152–278.
[90] M. R. Manaa, Int. J. Quantum Chem. **75**, 693 (1999).
[91] V. Kokoouline, O. Dulieu, and F. Masnou-Seeuws, Phys. Rev. A **62**, 022504 (2000); V. Kokoouline, O. Dulieu, R. Kosloff, and F. Masnou-Seeuws, *ibid.* **62**, 032716 (2000).
[92] O. Dulieu (private communication).
[93] J. T. Tellinghuisen, J. Mol. Spectrosc. **103**, 455 (1984).
[94] S. Kotochigova and E. Tiesinga, J. Chem. Phys. **123**, 174304 (2005).
[95] T. Bergeman, J. Qi, D. Wang, Y. Huang, H. K. Pechkis, E. E. Eyler, P. L. Gould, W. C. Stwalley, R. A. Cline, J. D. Miller, and D. J. Heinzen, J. Phys. B **39**, S813 (2006).
[96] J. B. Atkinson, J. Becker, and W. Demtröder, Chem. Phys. Lett. **87**, 128 (1982).
[97] Y. Wang, G. Wang, M. Li, and L. Li, Chin. J. Lasers **15**, 302 (1988).
[98] C. J. Williams and P. S. Julienne, J. Chem. Phys. **101**, 2634 (1994); L. P. Ratliff, M. E. Wagshul, P. D. Lett, S. L. Rolston, and W. D. Phillips, *ibid.* **101**, 2638 (1994); C. J. Williams E. Tiesinga, and P. S. Julienne, Phys. Rev. A **53**, R1939 (1996); E. Tiesinga, K. M. Jones, P. D. Lett, U. volz, C. J. Williams, and P. S. Julienne, *ibid.* **71**, 052703 (2005).
[99] H. Katô, M. Otani, and B. Baba, J. Chem. Phys. **91**, 5124 (1989).
[100] L. Li, Q. Zhu, and R. W. Field, J. Mol. Spectrosc. **134**, 50 (1989).
[101] E. Arimondo, M. Inguscio, and P. Violino, Rev. Mod. Phys. **49**, 31 (1977).
[102] W. T. Zemke and W. C. Stwalley, J. Chem. Phys. **100**, 2661 (1994).